

## CHAPTER 3

### ANALOGUE SITES AND THE MOON

#### 3.1 INTRODUCTION

From the literatures (Chapter 1) it was known that the moon can be divided into two types of rock dominant area: (i) anorthosite-suite of rocks dominant highland and (ii) basaltic-rocks dominant mare region. To understand the rock types on the lunar surface, it is necessary to understand their terrestrial analogues. It was observed that the lunar rocks have some analogues to the terrestrial ones. After reviewing the various rock types and



**Figure 3.1 Map of India showing locations of the lunar analogue rock sites**

their resemblance to the lunar counterparts, a few sites in India were chosen and they have been studied (Figure 3.1). In this chapter, a detailed study of the sampling sites, their geology, lithology and field relationships along with mineralogy and geochemistry are presented.

Field visits were made to Sittampundi complex, Chalk hills, Prakasam province (Highland analogue) and Deccan Plateau (Mare analogue) and rock samples were collected. Apart from rock samples, soils and ejecta samples (around Lonar region) were also collected to understand the regoliths, the space weathering products, since the lunar surface is impacted by many meteorites. In this study, a chondrite meteorite has also been used for the better understanding of the lunar surface.

### **3.2 TERRAE (HIGHLAND) ANALOGUE**

Lunar highlands are mainly composed of anorthosite, gabbroic anorthosites, anorthositic gabbros, gabbroic, noritic, troctolitic and dunite rocks (Tompkins and Heather 1997). In this study, most of the analogue rock types (except norite and troctolite) were collected from different parts of India.

The Highland analogue samples were collected from Sittampundi, Prakasam Province (anorthositic-suite), Chalk hills (dunite).

#### **3.2.1 Sittampundi Complex**

Sittampundi is located in Nammakkal district (Lat.  $11^{\circ}10' - 11^{\circ} 25'$  N and Long.  $77^{\circ} 50' - 76^{\circ} 05'$  E) of Tamil Nadu. The layered complexes occur in the Moyar-Bhavani-Cauvery tectonic zone in the form of tectonic slices (Selvan and Subramanian 2001). This layered sequence is called the Sittampundi complex after the village near its type exposure. The anorthosite

complex has been studied by many researchers include Nehru (1955), Naidu (1963), and Ramadurai and Sankaran (1970).

The complex consists of chromite-layered anorthosites with minor gabbros and ultrabasic rocks. They represent the rock types such as anorthosites, gabbroic anorthosites, anorthositic gabbros and gabbros similar to those of the moon. The Sittampundi anorthosite bodies associated with those of leuco-gabbro, pyroxenite, dunite and peridotite are traced along fractures and faults covering the Precambrian terrain in Tamil Nadu.

Windley and Selvan (1975) investigated the complex and discovered that it contains a primary igneous stratigraphy that passes upwards from rare pyroxenites, through gabbros, to anorthosites overlain by clinozoisite anorthosites in the northeast of the area. The Sittampundi complex (Windley et al 1981) is a metamorphosed anorthositic complex about 36 km long and 2 km thick (maximum) with an original igneous stratigraphy overprinted by high-grade metamorphic assemblages (Ramadurai et al 1975). The complete stratigraphy from top to bottom is (with maximum thicknesses): clinozoisite anorthosite (150 m), hornblende anorthosite (75 m) with several chromitite seams (6 m), and amphibolitic meta-gabbro (750 m) that contains layers of pyroxenite up to 100 m long.

The Sittampundi complex has a whole rock Sm–Nd isochron age of *ca.*  $2935 \pm 60$  Ma interpreted as the time of a first metamorphism soon after emplacement; a second high-pressure metamorphism at 11.8 kbar and  $830^\circ\text{C}$  (minimum) was inferred to have taken place at  $726 \pm 9$  Ma based on a whole-rock garnet–plagioclase–hornblende Sm–Nd isochron age of a garnet granulite in the Sittampundi complex (Bhaskar Rao et al 1996). The Sittampundi complex was formed and underwent metamorphism in the Neoarchaean, and was re-metamorphosed and re-deformed, together with other rocks in the suture zone in the Neoproterozoic–Cambrian, which we

interpret as the time when it was incorporated into the suture zone and the deep continental crust .

The complex is widest south of Sittampundi from where the belt thins, gradually veering to an east-north-easterly trend, straightening out again about 8km farther east near Karungalpatti, with uniform steep in the southerly

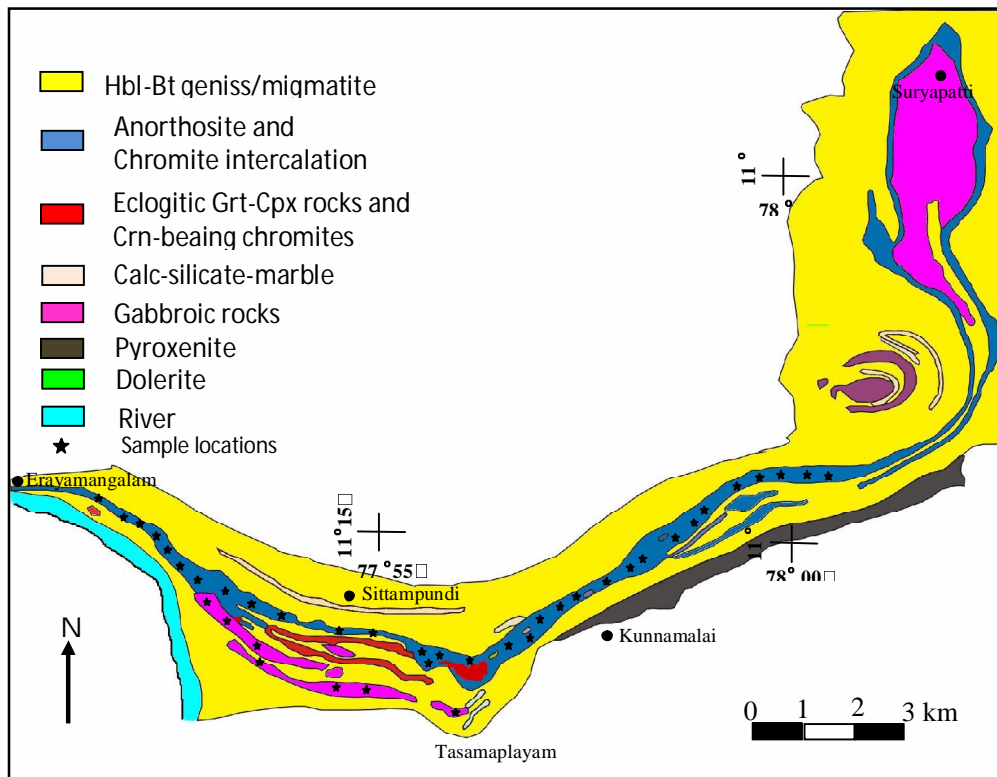


**Figure 3.2 Geological map of Sittampundi Anorthosite Complex  
(After Sanjeev et al 2009)**

dips of foliation. From Karungalpatti, this belt takes a sharp northerly trend in the form of an arc, ending 11km to the north near Suryapatti. Between Karungalpatti and Suryapatti the anorthositic rocks form individual bands of varying thickness making a number of small ridges and hillocks (Subramaniam, 1956). Many scientists and researchers (Mitra and Samanta

1996; Ramdurai et al 1975; Janardhana and Leake, 1975) have made extensive study about the Sittampundi anorthosites.

For this study, fieldwork was carried out in and around the Sittampundi, complex and rock samples were collected from sites. It was observed that the complex have well preserved igneous stratigraphy with the dunites/pyroxenites forming the residue, followed by garnet granulites, gabbros with orthopyroxene, gabbro, gabbroic anorthosites, chromite bearing anorthosites with the clinzoite bearing anorthosites occupying the uppermost horizon in the startigarphy similar to the observations by Selvan (1985) was fascinating. The samples were collected from the entire stretch of the belt (Figure 3.2). There were many abandoned quarries and recent work is also going around the region by GSI, as they found Platinum Group of Elements (PEG) around this complex (Satyanarayan et al 2007). The sample collection started from Irrumbupalam (Figure 3.3a) in the East to Cholasiramani (near) in the West. Along with the anorthosites, gabbroic anorthosites, anorthositic gabro were also collected from different parts of the belts including villages like Chinnapalayam, Kunnamalai (Figure 3.3b), Aikat, Kabilarmalai, Tasampalayam (Figure 3.3c), Karatupalam and near Sittampundi (Figure 3.3d). The rocks appears fresh, mostly white (anorthsoites), grey (anorthositc gabbro) to dark grey (gabbro). The layered complexes consist predominantly of anorthosite and leucogabbro with minor gabbro and ultramafic rocks, relict cumulate textures and graded mafic and felsic layers occur (Ramakrishnan et al 1978).

They can be distinguished from the surrounding biotite gneissic country rock by the mineralogy and texture i.e. the biotite gneissic rocks are composed of quartz, feldspar as major minerals and bitotite as major accessory. While the anorthosites are mostly composed of plagioclase with almost little or no quartz and hornblende ± pyroxene makes it to recognize on

the fields. Fresh samples were collected from well sites, abandoned quarries and also by removing the outer weathered surface from outcrops.

The distribution of the anorthosite is structurally controlled by the outcrops from Irrumbupalam to Tasamapalayam where the strike trends NE. From Tasamaplayam to Chinnapalayam strike is EW can be seen from the Figure 3.2. While the outcrop from Chinnapalayam to Cholasiramani it is SW. After collecting rock samples from the Archean anorthosite (oldest) from the Sittampundi complex, to understand the Proterozoic age anorthosites, Eastern Ghats granulites of the Andhra Pradesh were studied.

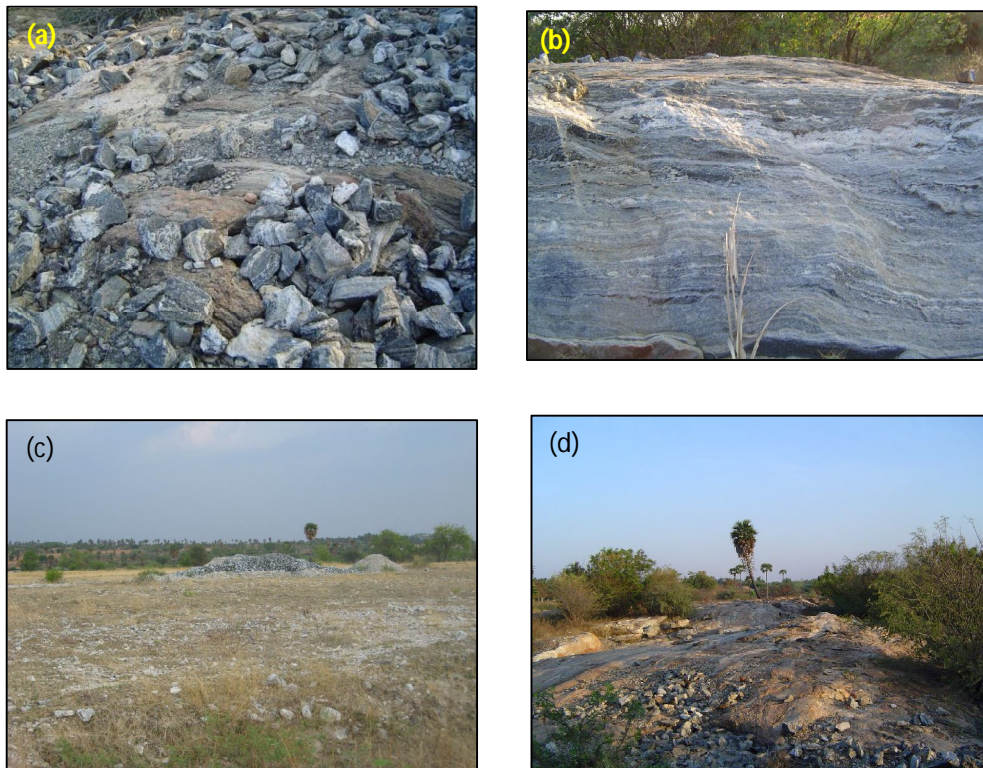


**Figure 3.3 Field photos of Sittampundi complex: (a) Irrumbupalam  
(b) Kunnamalai (c) Tasamplayam (d) Sittampundi outcrops**

### **3.2.2 Prakasam Province**

In the Prakasam District of Andhra Pradesh, south India both basic (gabbro-anorthositic) and alkaline bodies were emplaced at the junction zone of the Dharwar group of rocks and granulite rocks. The pluton comprises of gabbro, anorthosite, dykes of dolerite, lamprophyre, nepheline syenite, quartz syenite and rare anorthosite dyke, occurs at Boggulakonda, Settupalle, Purimetla, Pasupugallu, Chimakurti, Ravipadu and Kellampalle. Several of the isolated closures, particularly around Chimakurthi, Ravipadu and Pasupugallu, can be attributed to the gabbro–norite–anorthosite intrusive. Several plutonic rocks comprising gabbro–norite with some anorthosite and pyroxenites, are exposed around Chimakurthi (60 sq. km), Pasupugallu (60 sq. km) and Ravipadu (45 sq. km) (Figure 3.4a). All these plutons having an almost NE–SW trend lie west of the Krishna trough. It has been also established that the origin of these rocks is structurally controlled by reactivation of faults and correlated with seismic activity of the area (Swamy et al 2008). For the present study, rock samples were collected from Passupugallu, Ravipadu and Chimakurti sites.

#### **3.2.2.1 Pasupugallu plutons**

The Pasupugallu Gabbro Pluton, is an elliptical body (8×13 km) with NE-SW trending long axis, intruded the transition zone comprising amphibolite–granulite facies rocks of Ongole domain (Dobmeier and Raith 2003). The pluton consists essentially of gabbro and anorthosite with leucogabbro-norite as the subordinate unit. The dyke occurs as a sharply bounded planar body located about 3 km west of the village Turkapalem ( $15^{\circ}45'15''N$ ,  $79^{\circ}50'15''E$ ). The important country rocks include charnockites, khondalites, cordierite-sillimanite-biotite gneisses, granitic

gneisses and associated migmatites. The strike of foliation in the gneisses varies from NW-SE to NE-SW with predominant easterly dips (Nagaraju and Chetty 2005). The rock type comprises of anorthosite, gabbro, anorthositic gabbro and granites (Leelanandam and Reddy 1990). The Pasupugallu anorthosite belongs to Proterozoic age (Nagaraju et al 2008). In the field many small outcrops are seen but they are usually at ground level (Figure 3.4b).

Pasupugallu layered gabbro-anorthosite pluton located at the interface of a mobile belt and the craton to better understand its emplacement history and tectonic setting. The outcrops are scanty and are not much exposed in the central parts of the pluton, however, for this study few samples were collected from this pluton.

### **3.2.2.2 Ravipadu Gabbro Plutons (RGP)**

The Ravipadu Gabbro Pluton (RGP; 15°31'20N, 79°48'15"E) is a post-tectonic lopolith intruded into the Precambrian amphibolites. The pluton is elliptical in shape and covers about 40sqkm. The RGP is composed of abundant olivine gabbros, subordinate olivine norites and troctolites with significant anorthosites. In the field, anorthosites are better exposed than the gabbros due to the fact that they are more resistant to weathering (Kumar and Ratnakar 1996). There are two types of anorthosites: (a) cumulate anorthosites (CA) and (b) fractionated anorthosites (FA). The CA occurs as crescent shaped body within troctolites in the pluton and they are usually dark grey to black in colour, while the FA are sporadically present towards the peripheries of the pluton within olivine gabbros. They are usually light grey coloured with plagioclase feldspar.

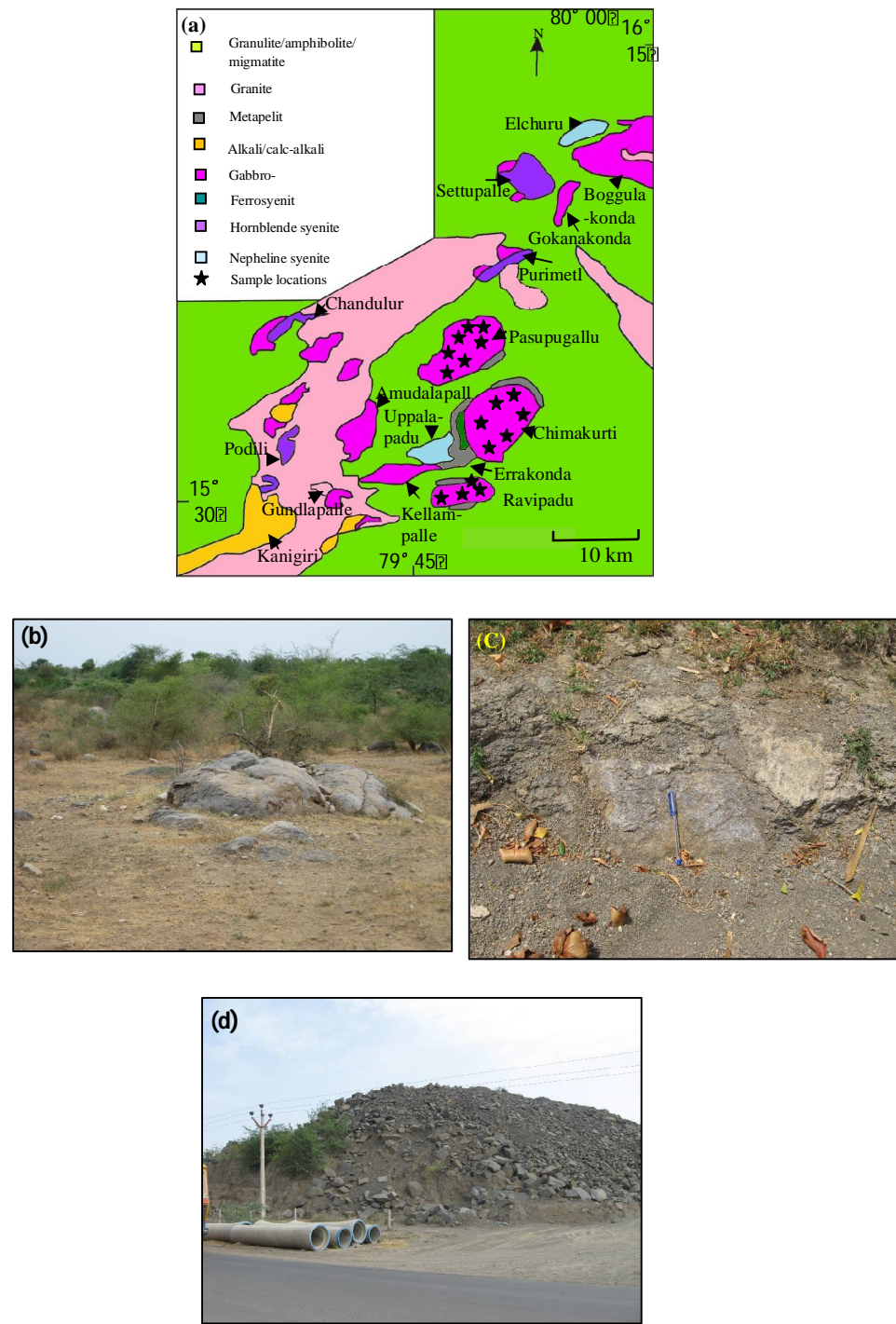


**Figure 3.4** (a) Geological map of Eastern Ghats alkaline rocks of Andhra Pradesh (after Kumar 2007) showing the sampling sites: Field photographs of (b) Passupugallu (c) Ravipadu (d) Chmiakurti sites.

The accumulation of early-formed plagioclase crystals along with minor mafic minerals has resulted in the formation of the CA and fractionation of mafic minerals from the parental basic magma has delivered the FA. Field evidences suggest that the CA is formed by crystal floatation. The CA and FA show textural diversity and variation in the mafic mineral content (Kumar and Ratnakar 1996). For this study field visit (Figure 3.4c), was made and observed that the anorthosites are well exposed as outcrops, they are light grey coloured (implies fresh) and the rock samples were collected from the site.

### **3.2.2.3 Chimakurti gabbro-anorthosite pluton (CGAP)**

The Chimakurti gabbro-anorthosite pluton (CGAP; 15°40'N, 79°50'E, Figure) in the Prakasam province (Figure 3.4d), contains a central olivine-clinopyroxenite, enveloped by a major gabbro-norite unit with intervening rock units which exhibit cumulate textures and they represent cumulates (Babu et al 1997). The Chimakurti pluton is concentrically zoned, and from core to margin consists of (1) olivine clinopyroxenite, (2) anorthosite, (3) olivine gabbronorite and (4) gabbronorite (Kumar et al 2001). The gabbros were collected from this site.

Kumar et al (2007) observed that the Chimakurti pluton appears concentrically zoned, with a sequence from core to margin of (i) olivine clinopyroxenite (ii) anorthosite, (iii) olivine gabbronorite and (iv) gabbronorite. The central clinopyroxenite may represent the early cumulates forming the base of the magma chamber, whereas the gabbronorites occupy the upper levels of chamber. At the contact with the Chimakurti pluton, metapelitic rocks record imprints of ultrahigh temperature contact metamorphism (>1000°C) at mid crustal conditions (~6-7 kb) (Babu 1996;

Dasgupta et al 1997). Two pyroxene thermometry records temperatures of ~1100°C at the centre of the Chimakurti pluton were also recorded. (Rao et al 1998).

The clinopyroxenite, anorthosite and gabbro portions of Chimakurti pluton show gradational relationships in terms of colour index and grain size in the field. Clinopyroxenite and anorthosite are coarse-grained (grain size up to 4 cm). There is a gradual decrease in the grain size from core to the periphery of the pluton (3-4 cm to <1 mm). Peripheral gabbronorite especially in the south-western margin, shows well-developed magmatic layering with inward dips of moderate to steep angles (72° to 78°; Babu 1996). Some of the marginal gabbronorites are very fine-grained (<< 1mm) and may represent chilled liquids. Locally, some of the marginal rocks show effects of strain including bending of plagioclase. High-Al gabbroic dykes are most common in the inner portions of the Chimakurti pluton. A rare hercynite accumulated band of 50 m length with a uniform thickness of 4 cm is reported within the leucogabbronorite from the Chimakurti pluton (Babu et al 1997).

### **3.2.3 Chalk Hills**

The ultramafic-ultrapotassic-carbonatites associations are uncommon, this rare association is found to occur along NE-NNE trending lineament (Tirupathur-carbonatite complex) and the ultramafic-syenite association is found along EW trending Arthur lineament in Tamil Nadu. At the intersection of these two lineaments, near Salem, Tamil Nadu dunite is found (Selvan 1981).

The Chalk hills (15 sq.km) are located in Salem district (Lat. 78° 5N Long. 11° 40E) of Tamil Nadu. Grady (1971) opine

d that the ultramafic rocks have been emplaced in the intersection of E-W trending 60 km long Godumalai shear zone and a N40 E trending about 25km long minor shear Srinivasan (1977). Kutty et al (1986) have shown that the Chalk hills complex is located as a continuation of the Bhavani shear. The emplacement of the complex is controlled by shears, which are deep crustal fractures (Grady 1971; Murthy 1979; Kutty et al 1986).

Middlemiss (1895) asserted that the ultramafics (Chalk hills) are essentially dunites with minor peridotite and noted the occurrence of chromite in the area. The complex is intrusive into the country rocks comprising gneisses, charnockites and garnetiferous mafic granulites. The complex is composed of two ultramafic bodies disposed in an en echelon pattern along ENE-WSW direction. The south-western part is almost composed of dunite and veins of hornblendite. The northern part is composed of dunite with patches of peridotites (Figure 3.5a). The dunites are fresh which is exposed by extensive mining (Figure 3.5b) of magnesite (Mohan et al 2000).

Though ultramafic rocks (in particular dunites) occur at many places (Salem to Omallur Road, Salem to Karupur Road) they are given a casual approach as they are highly altered due to extensive serpentinization and weathering. Fresh rocks are encountered only in quarries opened for magnesite at a depth of ten to twenty meters. For this study thirty two fresh dunite (unweathered) samples was collected from the northern part of the dunite belt.

The highland litho analogue samples collection complete with the Chalk hills. For the mare analogue Lonar basalt samples were collected.

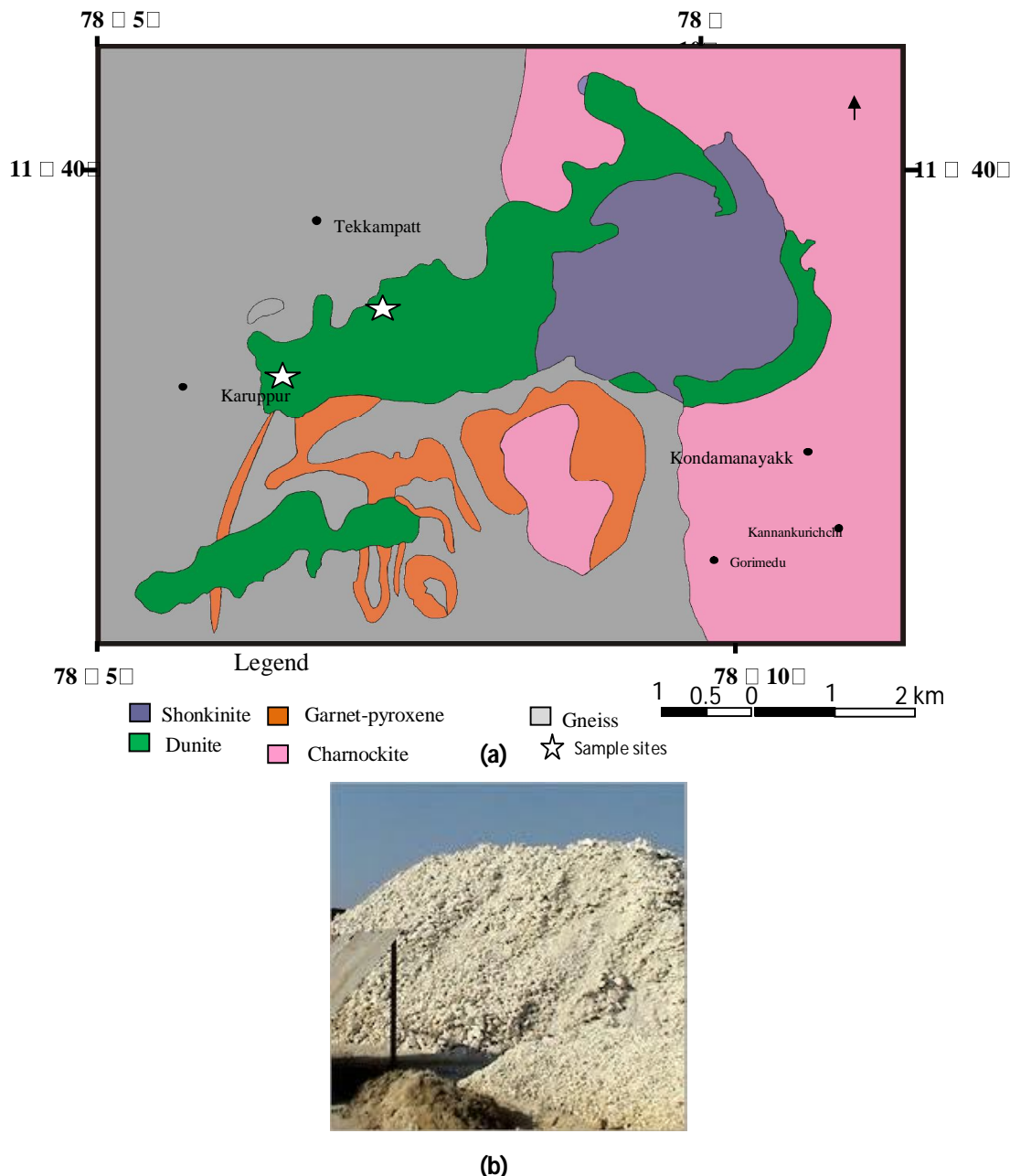


**Figure 3.5** Showing the (a) Geological map of Chalk hills, Tamil Nadu (after Mohan et al 2000) (b) Field photo of dunites in a quarry site

### **3.3 LOWLAND (MARE) ANALOGUE SITE**

The Deccan basalts rock samples were collected from Maharashtra in and around the Lonar for the mare analogue study. Because the Lonar represents a good analogue for impacts occurring on terrestrial-like bodies covered with primitive igneous rocks, such as the moon (Jourdan et al 2010).

#### **3.3.1 Lonar Geology**

Lonar Crater ( $19^{\circ}59' N$  and  $76^{\circ}31' E$ ) is a ~135 m deep, ~1.88 km diameter, near-circular depression in the Deccan Plateau of the Buldhana District, Maharashtra State, India. In terms of terrestrial impact craters the importance of Lonar Crater is that it is the only well-preserved simple crater in continental flood basalt and one of only very few in basaltic target rock in general (Nayak 1972; Fredriksson et al 1973). The depression contains at the bottom a shallow lake of saline water (Figure 3.6a). The chief constituent of the salt water is sodium carbonate, together with a small quantity of sodium chloride. These salts are thought to have been derived from the surrounding trap country by the chemical solution of the disintegrated products of the traps and subsequent concentration (Wadia 1966).

The origin of the Lonar lake hollow has been ascribed to a crypto-volcanic explosion unaccompanied by any lava eruption. This is one of the rare instances of volcanic phenomena in India thus the lake hollow is an explosion crater or a caldera. Another explanation is that the hollow is due to the impact of a meteorite which lies buried at some depth (Wadia 1966). Based on geomorphology and a variety of shock metamorphic features described, including the presence of shocked plagioclase with PDFs, maskelynite, and impact glass has been reported by many authors (La Fond and Dietz 1964; Nayak, 1972; Fredriksson et al 1973; Fudali et al 1980; Rao and Bhalla 1984; Ghosh and Bhaduri 2003; Koeberl et al 2004; Maloof et al 2010 and all the references there in) confirmed their impact origin.

The Lonar area, about 600-700 m of Deccan basalt flows overlies a Precambrian basement (Koeberl et al 2004). Thickness and nature of the basaltic sequence in Lonar is unknown (Kumar 2005). However Geological Survey of India (GSI) map (1993) indicates that there are about six flows inside the Lonar crater. Within the crater there are six 10 to 25 m thick basalt flows, all of which are characterized by broad flow fronts and nearly flat upper surfaces capped by discontinuous flow-top autobreccias. Within a single flow, an internal stratigraphy is usually developed that begins with thin, sporadically developed fine-grained pipe-vesicle basalt, followed by dense, non-vesicular, jointed and sometimes flow-banded basalts, which passes upward into vesicular, and sometimes amygdaloidal, fine-grained basalt that is often deeply weathered (Fudali et al 1980; Nayak 1972). The average slope of the inner wall is  $26^\circ$ , and the bedrock dips away from the crater at an angle of about  $8^\circ$  to  $20^\circ$  (Osae et al 2005). The Geological map of the Lonar crater is provided in Figure 3.6a.

During the field visit (May 2008), the Lonar crater (Figure 3.6b) was clearly seen without the hindrance of vegetation and samples were collected from the inner part of the crater near the salt lake to the outer part of the crater. Five individual flows of massive, vesicular and amygdaloidal basalts are exposed on the inner wall (Kumar 2005). Many rock samples from the Lonar crater and few ejecta (Figure 3.6c) and soil (Figure 3.6d) and also from quarry (Figure 3.6e) samples were also collected.

### **3.3.1.1 Lonar ejecta**

Ejecta of any crater are an important parameter to be studied because the way in which the ejecta is spread, tells about the angle of the meteoritic impact. Spreading pattern of the ejecta indicates degree of fluidisation of the rock and about the volatile components of the rock. This pattern also depends on the planet gravity and presence or absence of

atmosphere. Thus, if we know how these parameters affect the spreading of ejecta, then we can infer about the conditions of impact on that particular planet. The appropriate place to know these parameters is our earth itself (Misra et al 2010). However, hardly a few craters on the earth have been studied well with reference to this point. Lonar crater has surprisingly well-preserved ejecta (Figure 3.6c). Thus, these ejecta could be studied further.

The Lonar ejecta blanket is spread over about 1350 m away from the crater rim and slopes away by 2-6 degrees. The uppermost region of the ejecta contains the deposits that were melted due to the impact. The ejecta blanket also outcrops in small gullies, unlined wells, building foundation pits, trenches, and quarries. The ejecta blanket grades from overturned stratigraphy with brecciated units of several m sizes to unsorted clasts in a coarse matrix in the outer continuous ejecta (Stewart 2005). Similar observations were made during the field visit.

Ejecta located around the crater rim occur in two different forms (Fredriksson et al 1973, 1979). Most of the ejecta deposits are crudely stratified and unshocked, and contain clasts from a mixture of different bedrock units; these ejecta extend to within 1½ crater radii distance from the crater rim (Ghosh and Bhaduri 2003). A discontinuous overlying layer up to a meter thick is present in some places, which has clasts that are unshocked or show a range of shock effects up to intensely shocked varieties (planar deformation features in plagioclase and pyroxene and the presence of the high-pressure polymorph maskelynite; Kieffer et al 1976) and extends for ~½ crater radii km from the crater rim (Fudali et al 1980; Ghosh and Bhaduri 2003). Impact-derived melt rock fragments and glasses are common in the ejecta deposits up to about a crater radius from the crater rim and in the soil that is probably derived from the weathering of the ejecta (Nayak 1972; Fredriksson et al 1973; Ghosh and Bhaduri 2003). During this study ejecta

samples were collected from each direction (N, E, S, W) of the crater and the for further analysis (mineralogical, geochemical and spectral studies). The ejecta debris flow appears to be matrix supported with a nearly free-slip boundary. At the contact between the ejecta debris flow and the preimpact histosol, some histosol was incorporated into the flow, but the total contribution of secondary materials to the ejecta is not yet known.

The distribution of ejecta around the crater rim is informative regarding the direction and obliquity of the impact (Pierazzo and Melosh 2000; Herrick and Forsberg-Taylor 2003), but no unanimous opinion exists on the distribution of ejecta around the rim of the Lonar crater (Fredriksson et al 1973; Fudali et al 1980; Maloof et al 2005, 2007; Kumar 2005). Ghosh (2003), assuming a cometary impactor of ~90 m diameter and ~500 kiloton mass, suggested a direction of impact from the NW but provided no supporting data for this estimation (Misra et al 2010).

### **3.3.1.2 Lonar soils**

The uppermost basalt flow in this region is overlain in most places by a dense, structureless, black, clayey soil up to 2 m thick. This soil is exposed beneath the outer portions of the ejecta blanket in several gullies south of the crater (Misra et al 2010). Since not much details of the soil near the ejecta are available. In this study, soil samples were collected near the ejecta in the Lonar region (Figure 3.6d) and a comparative study was made between the soil, ejecta and the target rock. Thus the mare analogue basalt samples were collected from the Lonar (Deccan) region.

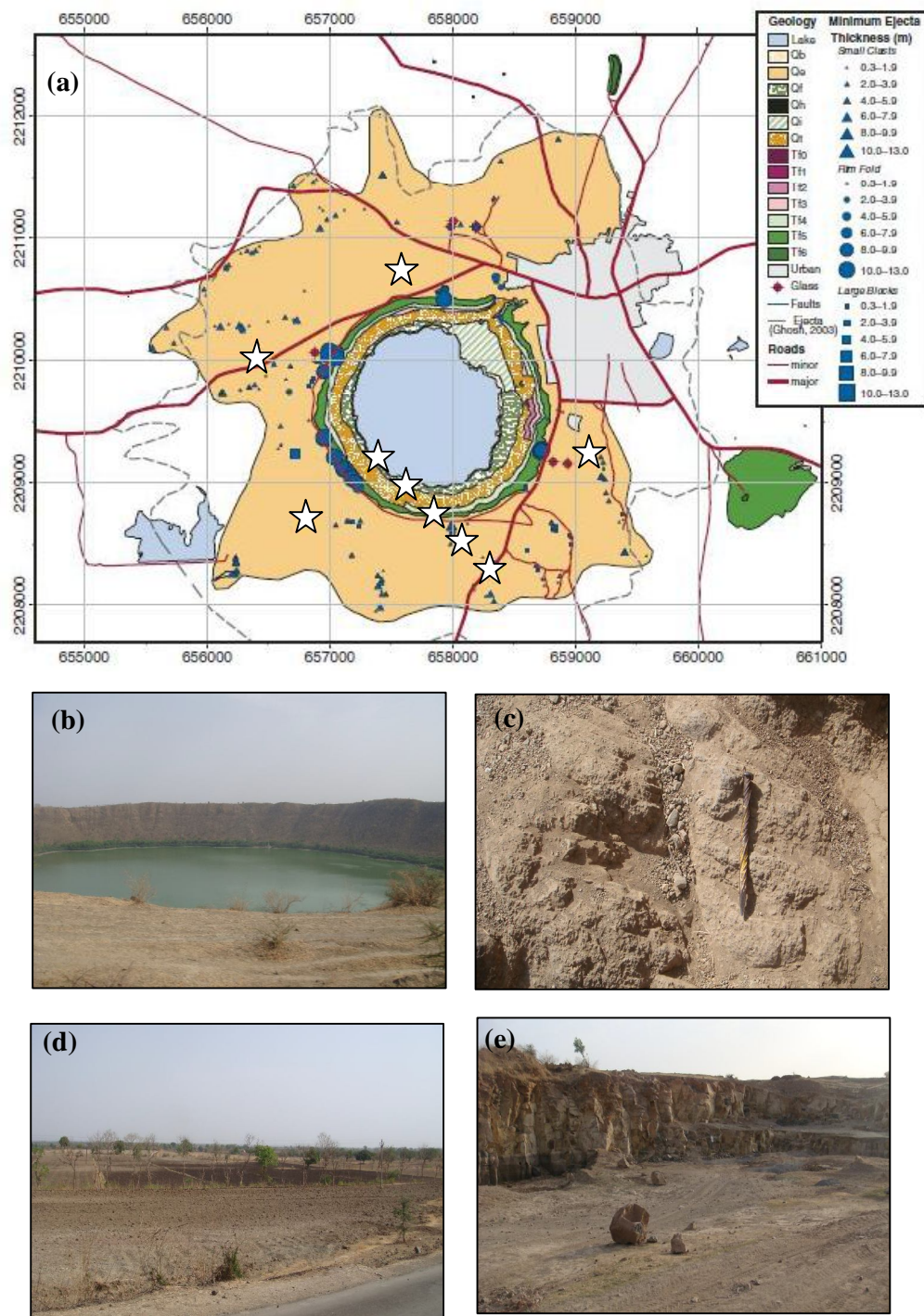


**Figure 3.6** Showing the (a) Geological map of Lonar crater (Source: Ghosh 2003): Field photographs (b) Lonar crater (c) ejecta blanket (d) soil (e) basalt quarry near crater Sample locations

### 3.4 METEORITIC COMPONENT

The moon is stable but heavily cratered surface provides evidence that is continuously bombarded by external objects. The projectiles that now enter the Earth/Moon system are derived from the asteroid belt and from comets. The term meteoroid is used for a naturally occurring solid body, travelling through space that is too small to be called an asteroid or a comet. It can be estimated that micrometeoroids of about milligram mass should be expected to strike lunar features, impacts by smaller objects will be more frequent, and by larger objects rarer. Although much is known about the size-frequency distributions of meteoroids, the consequences of these objects for prolonged space missions are still poorly understood (Heiken et al 1991).

It is believed that the space weathering (two process involved are micrometeorite bombardment and charged particle irradiation) processes create nanophase iron ( $\text{npFeO}$ ) (Noble et al 2007). It is important to determine the metal found in the lunar soil is actually extralunar in origin, having been brought in as a component of the meteoroids those have bombarded the moon over geologic time. Unfortunately, making distinction between the lunar and the meteoritic origin is a major problem and the results to date are controversial. Native iron metal,  $\text{Fe}^0$ , is rarely found in the terrestrial rocks, however in the lunar soils/regoliths they are mixed (as discussed in Chapter 1). The Apollo 16 soil contains about 2% input from the chondrite meteorite (Heiken et al 1991) in this study a recent fall meteorite in India has been studied in detail.

During the impact on the lunar surface it not only forms craters the deeper crustal rocks are excavated and exposed (in walls and as central peak) also ejecta materials. The projectile may be in most of the cases melted, vaporized or even ionized a part of the projectile will be part of remnant.

Samples of lunar impact melts collected from nonvolcanic surfaces are clearly the materials need for crater formation (Grieve 1982).

### 3.4.1 Sulagiri Meteorite

On 12<sup>th</sup> September 2008 around 8:30 hrs (Local time) the Sulagiri meteorite fell ( $12^{\circ}40'00''\text{N}$   $78^{\circ}02'00''\text{E}$ ) in the Krishnagiri district of Tamil Nadu, India (Weisberg 2009). The location of the meteorite fall located ~200 km from Chennai. According to GSI seven pieces of the meteorite were collected, totalling ~110 kg, making Sulagiri, the largest meteorite fall so far in India. The fragments fell in several locations like Addagurikki, Rauthapalli, Gangapuram and A.Kottur Villages of Hosur Taluk in Krishnagiri District (Figure 3.7a-d). Meteorites were recovered by the Revenue authorities of Krishnagiri District and handed over to the authorities concerned at the Geological Survey of India, Chennai, for further research and analysis. However, very few samples were recovered by the villagers.

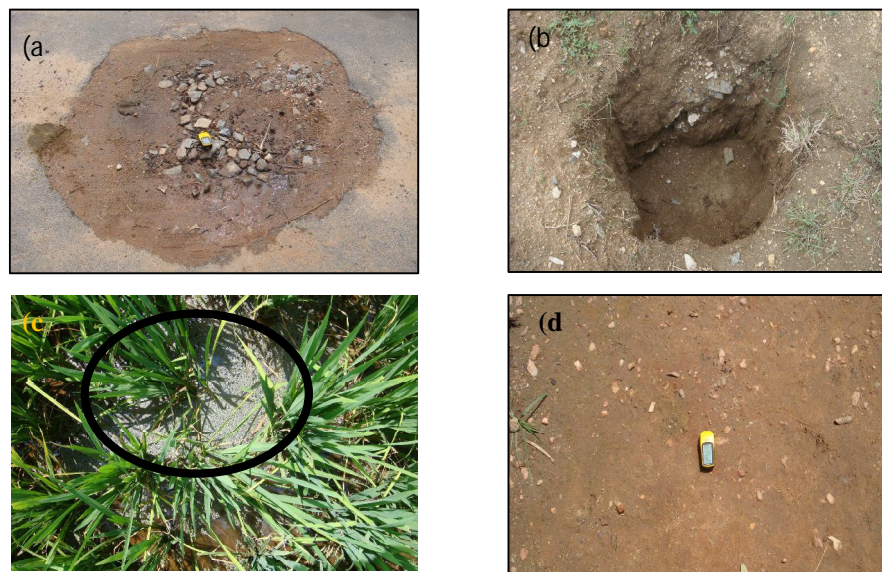


**Figure 3.7 Field photographs of the impact sites (a) Attakurkki crater  
(b) Gangapuram crater (c) A. Kothur(d) Rathupalli**

After the sample collections from all the five sites to identify and to know the mineralogy, megascopic and microscopic properties were studied in detail by comparing them with the published data of the moon.

### **3.5 PETROGRAPHY**

The Moon, like the Earth, is made of rocks. To learn about the Moon and its history, one has to learn something about lunar rocks- what they are made of, how they are studied and classified and how our experiences in interpreting rocks on the Earth have been applied to rocks on the Moon (Heiken et al 1991).

Minerals have provided the keys to understand rocks because their compositions and atomic structures reflect the physical and chemical and atomic structures reflect the physical and chemical conditions under which the rocks formed. Analyses of lunar minerals, combined with the results of laboratory experiments and studies of terrestrial rocks, have enabled scientists to determine key parameters are temperature, pressure, cooling rate, and the partial pressures of such gases as oxygen, sulphur and carbon monoxide- that existed during formation of the lunar rocks (Heiken et al 1991).

The moon is not a uniform, homogeneous planet. It consists of different rocks, formed in different ways at different times. Some of the Moon's rocks are familiar. The naming and classification of lunar highland rocks can be confusing, even for petrologists. The nomenclature is largely based on mineralogy (Hieken et al 1991).

The major rock forming mineral constituents of the lunar rocks include feldspar, pyroxene, and either olivine or a silica mineral. The rock types mostly represent feldspar-pyroxene-olivine or the feldspar-pyroxene-silica system. The rocks fall into four distinct groups: (i) the highland rocks,

(ii) basaltic (mare) volcanic rocks, (iii) breccias (iv) lunar soil/regolith (Hieken et al 1991). This study deals with highland, regoliths and mare rocks.

### **3.6 ANALOGUE SAMPLING**

The discovery of lunar anorthosite at Apollo 11 sparked comparisons with a variety of proposed terrestrial equivalents (Papike and Merrill 1980; Walker and McCallum 1982). Windely (1970) proposed an analogy between Archean anorthosites and the lunar anorthosites, in the same year Buddington (1970) drew an analogy between lunar and Proterozoic anorthosites. In this study too one such attempt has been carried out for lunar analogy studies.

Followed by the knowledge gained regarding the rock types on the moon from the lunar return samples and remote sensing data, similar rocks collection was made from different parts of India. From the field rocks samples were collected, to identify the rock type, two methods were followed first by hand specimen (megascopy) and second by thin section (microscopic) analysis. The properties like colour/colour index, texture, essential and accessory mineral, grain size (meagscopy), pleochroism, cleavage, fractures (microscopic properties) were studied.

This chapter deals with petrology, mineralogy, geochemistry and cosmochemistry of analogue rocks/samples collected from various locations/site, and they were compared with the published lunar counterparts. After sample collections, based on the observations made through hand specimen rocks were selected and categorised. Since the present study deals with the lunar analogues, weathered samples were omitted for further analysis.

### **3.7      SAMPLES STUDIED**

In this study samples, twenty nine anorthosites, ten gabbroic anorthosites and ten anorthositic gabbros of Sittampundi complex, six gabbroic anorthosites, four gabbros of Prakasam province, thirty two dunite samples of Chalk hills and one meteorite from Sulagiri were analysed. The sections and chemistry of major oxides of the samples is discussed in this chapter. The chemical composition obtained in this study was compared with those of the published chemistry and also with the lunar return samples chemical data.

To understand and to identify lunar analogue one can correlate terrestrial rock's properties like chemical and mineralogical composition to term a rock as anlaouge.

Apart from the rocks the lunar soil that covers most of its surface is formed due to meteoritic impact. It results in reduction of grain sizes and secondly (rare) mixing of the meteoritic component. To understand the lunar regoliths a simulation study has been carried out by selecting one sample from each category (highland- anorthosite, gabbroic anorthosite, anorthositic gabbro; mare- basalt) were prepared via crushing and powdering the sample (Chapter 1). Apart, naturally occurring basalt soil and ejecta (impact) were also collected from Lonar region. Heiken et al (1991) determined that about 2% of chondritic meteoroids were observed from lunar return samples. Hence, in this study a meteorite also included.

#### **3.7.1    Highland Lithology and Analogue Rocks**

The highland is composed of various plutonic rocks. Classification for highland rocks is roughly parallel to that for similar terrestrial rocks. They are divided into several groups. The rock types include anorthosite, gabbroic-

noritic-troctolitic anorthosite, gabbroicnoritic- troctolitic anorthosite, anorthositic norite, anorthositic gabbronorite, anorthositic gabbro, norite, gabbronorite, gabbro, anorthositic troctolite (Tompkins and Heather 1999) and duntie (Hieken et al 1991).

There are many types of anorthosites which include, alkali, Mg-rich, ferron. Ferron anorthosites are rocks are light-coloured, rich in Ca and Al, and are composed mostly of plagioclase feldspar. Minor minerals include pyroxene and olivine, which are richer in Fe than those of most Mg-rich crustal rocks. Hence the adjective ferroan is applied to these anorthosites. These anorthosites may be the products of flotation of plagioclase in a magma ocean.

Alkalic rocks from the highlands of the Moon, though relatively minor in volume, yield important information in understanding the later development of the lunar crust. Mineralogically and chemically more evolved lithologies, such as granites and felsites, have been known from the Moon since the earliest days of the Apollo lunar sample returns (Brown et al 1972). Early work on returned lunar rocks also identified samples of what turned out to be more typical high lands lithologies, especially anorthosite, which have anomalously high alkali element contents (Hubbard et al 1971). Highland Anorthositic Suite (HAS) plutonic rocks include granites, rhyolites, felsites, and quartz monzodiorites. HAS gabbros, norites, and gabbronorites, by definition, exhibit a much broader spectrum of mineralogical diversity, yet are essentially plagioclase-rich mafic cumulates.

Mg-rich rocks, forms the second group of rocks is more varied, including some plagioclase-rich rocks, but many rocks with more pyroxene and olivine and correspondingly smaller amounts of plagioclase. Within the Mg-rich group are several rock types distinguished by their major minerals. Gabbros and norites are composed of pyroxene and plagioclase, troctolites

contain mostly olivine and plagioclase and dunites are nearly pure olivine rocks. If a magma ocean did indeed form on the moon, the Mg-rich rocks probably formed after it had largely solidified. Other rock types of highland include KREEP, breccias (Heiken et al 1991) are also present.

The study of ultamafics has been drawing the consistent attention of geologists for a long time as they are the representatives of the mantle which is inaccessible to direct investigations (Selvan 1981). It was also observed that lunar's dunite may have originated from a considerable deeper depth of 10-30 km. There has been very less studies carried out for correlation between earth and moon dunites. Hence, during this study Chalk hills dunites were compared with the lunar dunites. This may be the first work to correlate the Chalk hills dunite with those of the moon.

An understanding of the composition and evolution of planetary crusts has been one of the major objectives of planetary science. Studies of the suite of returned Apollo and Luna samples readily led to the recognition that large-scale lunar differentiation occurred early in lunar history (Taylor 1982). One common scenario includes a magma ocean, hundreds of kilometres deep that formed from the heat of late-stage accretion and intense bombardment. Plagioclase feldspar and mafic cumulates crystallized or aggregated from this resulting mush forming the earliest lunar crust and mantle, respectively. In the first 700 million years of lunar history several chemical and physical processes were involved in forming or altering the lunar crust, only portions of which were to be sampled 3.8 billion years later. Some of these processes are well-documented (the major basin-forming impacts; derivation of mare basalts from mantle cumulates). Other processes are less well defined but are required in some form in order to account for the nature and variety of lunar crustal materials. For example, after differentiation of the ultramafic mantle and feldspathic crust, Mg-rich magmas generated

perhaps by partial melting of the mantle or the deeper interior are hypothesized to have intruded the lower (Warren and Wasson 1980) or entire (James 1980) crust, where they formed layered plutons (composed mostly of noritic rock overlying troctolitic rock, dunite and others).

### **3.7.2 Anorthositic-suite of Rocks**

#### **3.7.2.1 Lunar anorthositic-suite of rocks**

An understanding of how the lunar crust formed requires knowledge of the composition and distributions of rock types within the crust. Even after decades of study, new rock types continue to be discovered primarily through studies of clasts from breccias and soils (Norman et al 1991). Lunar highlands are mainly composed of anorthosite, gabbroic, noritic, or troctolitic rocks (Tompkins and Heather 1997).

There are broadly three types of lunar anorthosites. They are Alkaine, Mg-rich and Ferron anorthosites. Alkaline anorthosites are generally granular and cataclastized, not unlike their more Ca-rich cousins the FANS. In addition to plagioclase, some of which retains its original coarse grain size ( $> 1$  mm), cumulate texture, HAS anorthosites contain minor amounts (generally  $< 5\%$ ) of ilmenite and high-Ca pyroxene (Lindstrom et al 1988; Warren et al 1990; Snyder et al 1992). Olivine is conspicuously absent in HAS anorthosites, whereas it is a common constituent of FANS. A few HAS anorthosites also contain whitlockite (Warren et al 1983; Snyder et al 1992).

In this study Lunar return samples were compared with those of terrestrial rocks collected from various sites. The lunar alkaline anorthosite sample number 14304 is a white/light coloured and composed of plagioclase (90%) with very low pyroxene content (Goodrich et al 1986). Large plagioclase grains (1-2 mm) from within the anorthositic portion are uniformly less calcic ( $\text{An}_{72-83}$ ). High-Ca pyroxene in the anorthositic portion is minor

and relatively fine-grained (<0.2 mm). Low-Ca pyroxene appears to be nonexistent (Snyder et al 1995).

The plutonic rocks of the magnesian suite (Mg-suite) represent the period of lunar basaltic magmatism and crustal growth (4.46 to 4.1 Ga) that immediately followed the initial differentiation of the moon by Magma Ocean (MO) formation and crystallization. The volume and distribution of the Mg-suite and its petrogenetic relationship to latter stages of lunar magmatism (mare basalts) remains obscure. These plutonic rocks exhibit a range of compositions and include ultramafics, troctolites, spinel troctolites, norites, and gabbronorites. A distinguishing characteristic of this suite is that they contain some of the most magnesium-rich phases ( $\text{Fo}_{95-90}$ ) that had crystallized from lunar magmas (Shearer and Papike 2005).

Mg-rich rocks: this second group of rocks is more varied, including some plagioclase-rich rocks, but many rocks with more pyroxene and olivine and correspondingly smaller amounts of plagioclase. Within the Mg-rich group are several rock types distinguished by their major minerals. Gabbros and norites are composed of pyroxene and plagioclase and dunites are nearly pure olivine rocks. If a magma ocean did indeed form on the moon, the Mg-rich rocks probably formed after it had largely solidified.

The Mg anorthosite sample number 76504,12 is composed of anorthosite (90%) and pyroxene (10%) (Synder et al 1995) was used in this study for comparison.

The ferron anorthosite sample number 15415 is made up of 98% plagioclase, with minor pyroxene and trace ilmenite and silica. The maximum grain size of plagioclase in 15415 is 1.8 cm (Wilshire 1972), or 3 cm (James 1972) with crystals grown together with smooth grain boundaries and trigonal intersections (typically a metamorphic texture). Stewart et al (1972) coined

the term Apollonian metamorphism to describe the texture of plagioclase and mineral assemblage of 15415. Minor diopsidic augite (Ca-pyroxene) occurs as inclusions in plagioclase, polygons along grain boundaries and septa between large plagioclase grains. The pyroxene grains are small (~100 microns) and show exsolution of pigeonite and orthopyroxene (Figure 3.8a). For this study this sample was used for comparison.

The lunar Clasts of gabbroic anorthosite sample 67455 have a range of texture from coarse granoblastic to fine-grained hornfelsic (Minkin et al 1977). It is composed of plagioclase (51-75%), pyrozene (8%), olivine (4%), opaque (3-5%) (Meyer 2010). The Lunar gabbros anorthositic (Figure 3.9a) contain subidiomorphic to idiomorphic plagioclase, olivine and rare clinopyroxene phenocrysts in a mafic groundmass. The anorthosite and anorthositic gabbro fragments are products of fractional crystallization under plutonic, hypabyssal or stagnant volcanic conditions (Woods et al 1970). For this study this sample was used for comparison.

Gabbroic rocks are of particular interest to lunar scientists because they are not well represented in the lunar sample collection, and yet are expected on the Moon for several reasons. Within the impact craters Aristarchus, Bullialdus, and Tycho, where gabbroic plutons may have been exposed as a result of the impact process (Tompkins et al 1999)

The lunar anorthositic gabbro/gabbro sample 77017 is a coarse-grained poikilitic (or poikiloblastic) texture (Helz and Appelman (1974), McCallum et al (1974), Ashwal (1975), McGee et al (1979), Meyer (1994), Cushing et al (1999) and Hudgins et al (2008)). The rock is composed of plagioclase (75%) shows twining, undulatory extinction, with high Ca-pyroxene (augite) and also low Ca-clinopyroxene (10%) were reported by Hudgins et al (2008) and McCallum et al 1974 also little olivine (5%) and ilmenite is also present (Figure 3.10a). This sample was used for comparision.

The highland comparision rocks include Sittampundi anorthositic-suite of rocks, Prakasam Province anorthositic-suite were made. Mineralogy and geochemistry were determined and they were compared with the lunar counter parts.

### **3.7.2.2 Sittampundi anorthositic-suite of rocks**

The Sittampundi complex in Tamil Nadu is one of the best documented Archean calcic anorthosites and has been studied in detail by Subramanian (1956) and latter by Janardhan and Leake (1975). The complex according to Windley and Selvan (1975) is comparable with the Fiskenesset Complex of Greenland. The complex is arcuate shaped extending for nearly 20 km and is about 1.5 km wide in the central portion. The rocks contains linear bands and lenses of garnetiferous mafic granulites which according to Subramanian (1956) are enigmatic rocks. Further, Chappell and White (1970) carried out mineral analysis on the garnet and clinopyroxene and found that the clinopyroxene is not omphacite but contains only ~1 wt% soda. The P-T estimates made shows that the rocks were metamorphosed at 850°C at 7-8 kbar and is well within the field of granulite facies metamorphism.

Anorthosites are the predominant rock type in the Sittampundi complex and are exposed at many places as out crops in the field. A detailed study of the country rock (biotite gneiss) in this region was beyond the scope of this project.

Anorthosite occurs as cumulate layers from a centimetre or so to few hindered meters thick at different horizons in layered basic plutons. In layered basic plutons anorthosites occur at all levels of segregation bands in mafic rocks.

In hand specimen, the anorthosites can be identified as they contain abundant plagioclase (85-90%), with little mafic minerals. They are usually medium-coarse grained. They are usually light coloured (leucocortic) few samples are associated with layers of chromite. For this study, fresh rocks (29 samples) were selected for further analysis. While the thin sections (Figure 3.8c-f) shows that the anorthosites are equidimensional and euhedral to subhedral, contain very calcic plagioclases, in the range  $\text{An}_{90-100}$  in addition to more typical  $\text{An}_{75-85}$  compositions with cumular texture.

The plagioclase-rich rocks have about 50 to 95%  $\frac{1}{2}$  to 2mm lamellar-twined plagioclase, the composition lies between  $\text{An}_{85}$ - $\text{An}_{95}$ . The other major constituent is pale green hornblende these two minerals occurs in a granular texture usually with triple junctions that are taken to be an equilibrium metamorphic texture. Minor clinopyroxene, clino-pyroxene occurs as accessory minerals. Triple junction textures mainly involve plagioclase, hornblende and clinopyroxene (Janardhanan and Leake 1975).

The amphibole is hornblende formed as recrystallized primary igneous hornblende or was derived by metamorphic reaction of pyroxene, olivine, plagioclase and water the evidence is not decisive (Leelandam 1987).

The second abundant rock in the Sittampundi complex are gabbroic anorthosites. The gabbroic anorthosite is made up of plagioclase ( $\text{An}_{80-100}$ ) more than 75-80%, pyroxene (10%) and hornblende (5-10%). exhibits coarse grained, size varies between 2-2.5mm in length, dark coloured, massive in hand specimen. While the thin section (Figure 3.9b) shows subhedral plagioclase (>85%), hornblende (20%) and rest opaques and trace minerals like zircon. The plagioclase show twinning, triple junctions are common (Figure 3.9b). Hornblende shows pleochroism from pale green to green.

Ramadurai et al (1975) considered the possibility of the anorthositic gabbro/gabbro that it might be unrelated genetically to the anorthosites, but the fact that about 30 cm above the contact with the garnet-bearing gabbro there are layers of similar gabbro in the anorthosites points to a primary igneous stratigraphic relationship between these rock groups. The gabbros are commonly well-layered with plagioclase and mafic minerals in the anorthosite zones. The clinzoisite is typical in the compositional. The rock contains coarse and zoned labradoritic plagioclase, pyroxene and hornblende also iron oxides (magnetite) as accessories.

The Sittampundi anorthositic gabbros are commonly well-layered with plagioclase and mafic minerals in the anorthosite zones. The clinzoisite is typical in the compositional (Ramadurai et al 1975). The rock contains coarse and zoned labradoritic plagioclase (70-75%), pyroxene (20%) and hornblende (5-10%) and remaining iron oxides (magnetite) as accessories (Figure 3.10b).

The plagioclase are lamellar-twin plagioclase, the other major constituent is pale green hornblende and Ca-rich pyroxene. These minerals occur in a granular texture usually with triple junctions that are taken to be an equilibrium metamorphic texture. Minor clinzoisite, clino-pyroxene occurs as accessory minerals. Triple junction textures mainly involve plagioclase, hornblende and clinozosite similar to that observed by Janardhanan and Leake (1975).

Since the present study deals with the analogue study of the moon, anorthosites, gabbroic anorthosites, anorthositic gabbros/gabbros were considered for further studies.

### **3.7.2.3 Prakasam Province Anorthositic-suite of Rocks**

The second study site was the Prakasam province (Andhra Pradesh) where the anorthositic-suite of rock samples was collected from the Pasupugallu, Ravipadu and Chimakurti plutons complex. The complex mainly exhibits gabbroic anorthosites, anorthositic gabbro/gabbro rock types.

The Passupugallu gabbroic anorthosites are medium grained, hypidiomorphic, with plagioclase content ranging from 65–85%. Plagioclase grains are deformed, showing bent twin lamellae, and feeble zoning is observed in some untwinned crystals. Sometimes, biotite forms discontinuous rims around opaques. These are very coarse grained, mostly massive, with feeble alignment of minerals at places. Plagioclase is the dominant mineral with minor clinopyroxene, olivine and biotite. Triple junctions can be observed among subhedral plagioclase crystals (Figure 3.9c).

The Passupugallu gabbros consist predominantly of plagioclase, clinopyroxene and biotite, with minor orthopyroxene, opaques and rarely olivine. The magmatic fabrics of gabbros are characterized by hypidiomorphic, cumulate and subophitic textures with plagioclase, augite and biotite as the essential minerals, and spinel, opaques, apatite as accessories. Olivine is conspicuous. Plagioclase grains are subhedral and display albite and Carlsbad-albite twinning, which are deformed in places. The gabbros at the southern part of the pluton are relatively finer-grained and more deformed, preserving peripheral granulation, bent, and kink twin lamellae. Augite is subhedral with exsolution lamellae of orthopyroxene, ilmenite needles, and rarely having olivine and plagioclase inclusions with biotite rims. Grain boundaries are lobate, sometimes straight and rarely deformed. The lattice preferred orientation of plagioclases and clinopyroxenes in magmatic stage is shown in Figure 3.10c.

The Ravipadu gabbroic anorthosites show dark grey colour plagioclase with medium grained texture in hand specimen. Thus it may be considered as the samples as Cumulate anorthosite (CA) type rather than Fractionated anorthosites (FA). In thin section it exhibits cumulate texture, composed of plagioclase, olivine, orthopyroxene, clinopyroxene and rarely opaque oxides. The plagioclases are euhedral to subhedral and contain microlites of magnetite. The plagioclase-olivine interface is often marked by thin rim of orthopyroxene and rarely by clinopyroxene. The anorthite content range from  $An_{72}$ - $An_{67}$ . Olivine is subhedral and few are irregular shapes. Orthopyroxene is anhedral and shows pinkish brown to light green pleochroism. Clinopyroxene occurs as corona around olivine. It is pinkish brown in colour (Figure 3.9d).

The gabbro megascopically is melanocratic, compact, dense and exhibits metallic lustre. The grain size ranges from 3mm to 5 mm. The thin section shows presence of plagioclase, olivine, clinopyroxene and orthopyroxene as major mineral constitutions while amphibole and opaque oxides form the minor minerals.

The plagioclase is mostly unzoned, clouded and turbid, Anorthite ranges from  $An_{46}$ - $An_{70}$  (Kumar and Ratnakar 1995). Clinopyroxene are moderately pleochroic (green to yellow), may be augite or diopside. orthopyroxene is pleochroic from pink to light green (Figure 3.10b).

Thus the anorthosites are mostly composed of plagioclase feldspars, as the mafic content increases it is gabbroic anorthosites and gabbros. The Prakasam province composed of plagioclase and pyroxenes, this indicates not much of weathering or alteration has occurred in the region.

To understand the origin, chemical analysis are essential.

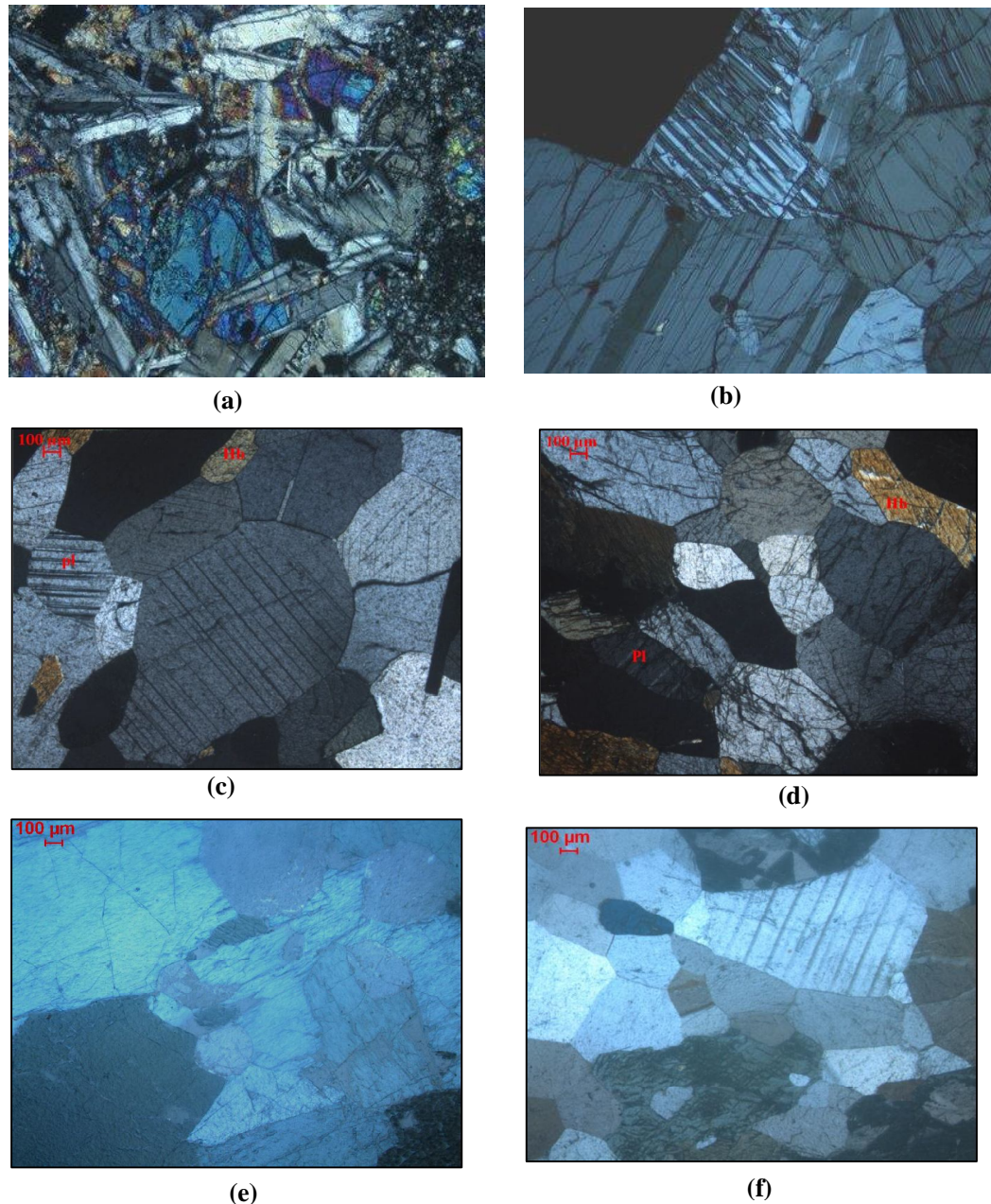


**Figure 3.8 Thin sections photographs of Anorthosite (a) Lunar alkaline -14304,165 (b)Lunar Ferron – 15415 (Lunar : Source: Lunar atlas- LPI) (c-f) Sittampundi**

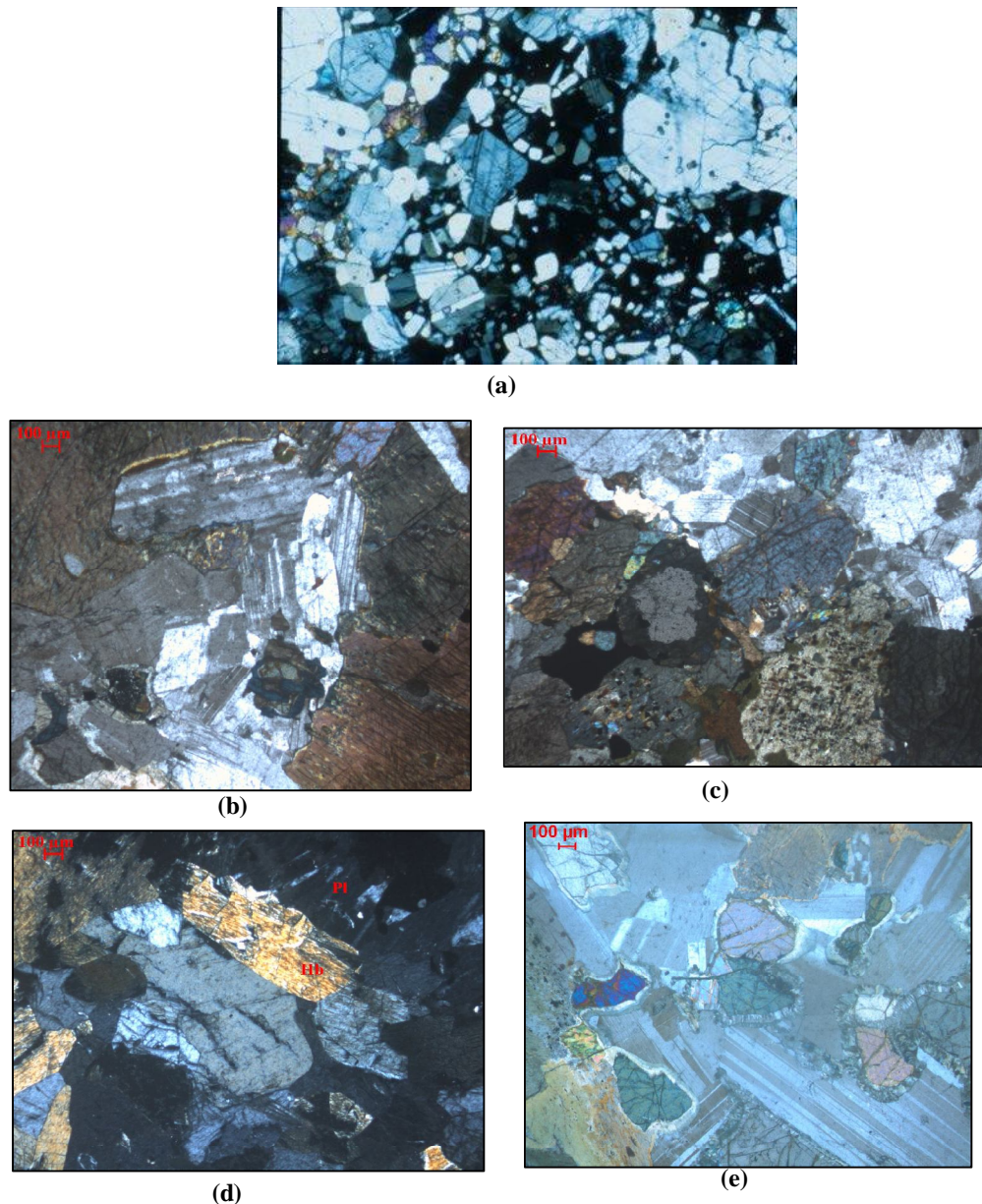


**Figure 3.9 Thin section photographs of gabbroic anorthosite**  
**(a) Lunar- 67455 sample (Lunar : Source: Lunar atlas- LPI)**  
**(b) Sittampundi complex (c) Passupugallu pluton**  
**(d) Ravipadu pluton (e) Chimakurti pluton**

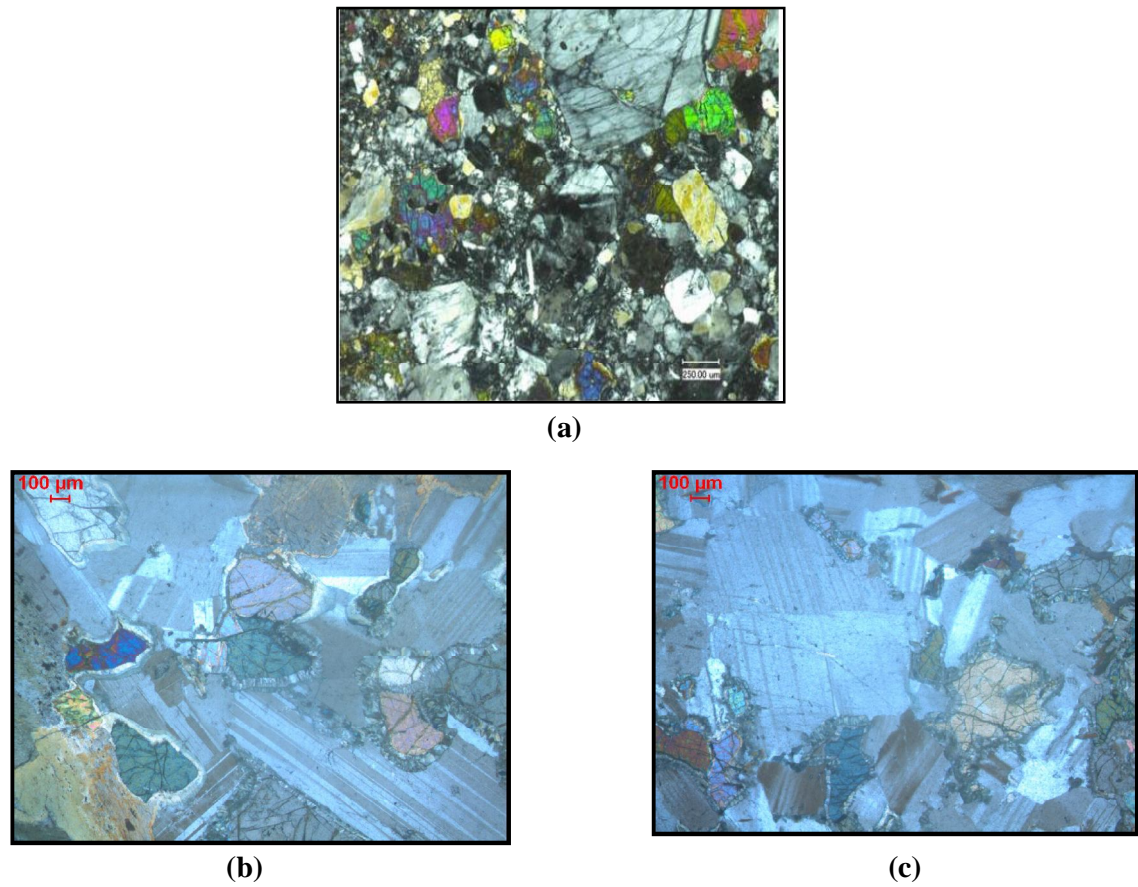


**Figure 3.10** Thin section photographs of anorthositic gabbro/gabbro (a)  
**Lunar anorthositic gabbro Apollo sample No77017 ((Lunar**  
**: Source: Lunar atlas- LPI) gabbro (b) Sittampundi complex**  
**(c) Praksam province**

### 3.7.3 Chemical Correlation between the Earth and Moon Anorthositic Rocks

Twenty nine anorthosites (Sit-A), ten gabbroic anorthosites (Sit-GA) and ten anorthositic gabbros (Sit-AG) of Sitampundi complex, four gabbroic anorthosites (AP-GbAn), five gabbros (AP-AG/G) of Prakasam

province have been analysed and the results are given in Table 3.1 along with the published data of the same site and the lunar sample.

Table 3.1 shows the major oxide geochemical data of anorthosites (Sittampundi An1-A29: compared with Janardanan and Leake (1975) T- L (Sit-Com-A) 1975; Lunar Alkaline anorthosite sample no. 14304; Lun -AlK Lunar Mg-suite anorthosite sample no. 76504,12 (: Lunar Ferron anorthosite sample no. 15415). Gabbroic anorthosite (Sittampundi GbAN1-10; Pasupugallu Pas-GbAn1; Ravipadu Ravi-GbAn 1-2) is provided in Table 3.2. Anorthositic gabbro/gabbro (Sittampundi Sitam-AnGb/Gb1-10; Passupugallu Pas-AnGb/Gb 1-2; Ravipadu Ravi-AnGb/Gb1-3) is given in Table 3.3.

The major elements/oxides analysis methods of the anorthositic suite of rocks include, alkaline-sub-alkaline classification, ACF diagram, AFM diagram, Harker variation diagram between  $\text{SiO}_2$  and other major oxides

### **Alkaline diagram**

The silica-alkalies variation diagram of Figure 3.11 can be used to subdivide all igneous rocks graphically into two categories – alkaline and sub-alkaline. Alkaline rocks have relatively high concentrations of alkalis (Na, K) relative to silica, so that usually they are undersaturated and have normative nepheline. These chemical properties such as alkali feldspar, feldspathoids, alkali-rich pyroxenes, and alkali-rich amphiboles. Ca-poor pyroxene (hypersthene) is never found in alkaline rocks. The most common alkaline rocks belong to the alkali olivine basalt suite, comprising basalts as well as more felsic rock types (Lake 2008).

While the subalkaline rocks have higher silica relative to alkalis and consequently generally have orthopyroxene or quartz in the norm and never

feldspathoids. Subalkaline rocks may be further divided into the tholeiitic suite and the calc-alkaline suite. The tholeiitic suite, comprised primarily of basalts but including more felsic rocks (Lake 2008).

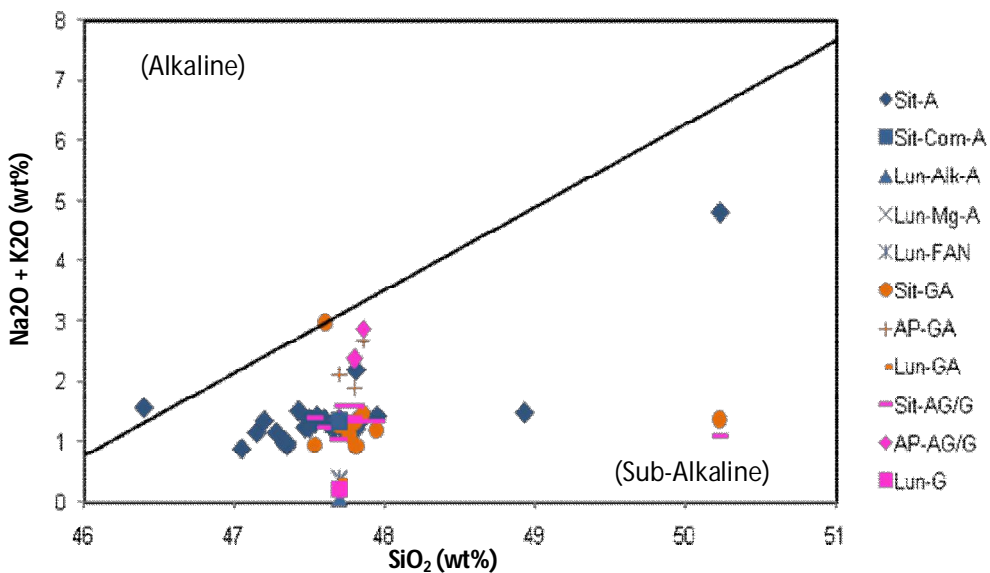


**Figure 3.11 Alkaline-subalkaline diagram (modified after Oslo 1992)**

The calc-alkaline suite comprises the common volcanic basalt-andesite-dacite-rhyolite and plutonic gabbro-diorite-granodiorite-granite associations, which contain combinations of olivine, Ca-rich clinopyroxene, Ca-poor orthopyroxene, hornblende, biotite, feldspars and quartz (Lake 2008). The samples (including anorthosite, anorthositic gabbro and gabbro of both terrestrial and lunar) studied belongs to sub-alkaline suite (Figure 3.11).

**Table 3.1 Whole rock major oxides wt (%) of terrestrial and Lunar (alkaline, Mg-rich and Ferron) anorthosites**

Oxides wt (%)	A1	A2	A3	A4	A5	A6	A7	A8	A9	A10	A11	A12	A13	A14	A15	A16	A17	
SiO <sub>2</sub>	47.70	47.85	47.80	47.54	50.22	47.95	47.60	47.81	47.76	47.71	47.69	47.27	47.66	46.40	48.93	47.20	47.54	
Al <sub>2</sub> O <sub>3</sub>	27.11	29.71	27.26	27.08	22.39	28.42	24.80	25.19	23.35	22.98	27.17	24.36	25.69	24.55	25.27	20.60	25.20	
TiO <sub>2</sub>	0.58	0.50	0.52	0.51	0.50	0.52	0.54	0.54	0.54	0.54	0.51	0.56	0.51	0.52	0.10	0.11	0.13	0.53
Fe <sub>2</sub> O <sub>3</sub>	6.49	3.21	4.71	3.88	2.97	4.44	6.40	5.26	7.49	7.92	5.56	4.03	5.44	4.10	2.58	4.91	6.27	
MnO	0.09	0.05	0.07	0.05	0.04	0.06	0.08	0.07	0.10	0.10	0.07	0.06	0.07	0.05	0.04	0.07	0.14	
MgO	2.49	0.93	2.65	1.29	0.31	2.31	3.94	3.42	4.94	5.52	2.08	2.29	3.85	7.35	4.24	9.53	2.84	
CaO	15.44	16.71	15.81	15.86	7.13	16.22	14.86	14.95	14.79	14.35	14.86	14.97	15.40	14.63	15.35	14.47	14.61	
Na <sub>2</sub> O	1.34	1.38	1.29	1.28	2.83	1.39	1.29	1.17	1.22	1.18	1.33	1.14	1.19	1.52	1.40	1.31	1.40	
K <sub>2</sub> O	0.03	0.01	0.02	0.02	1.98	0.02	0.03	0.04	0.02	0.02	0.01	0.00	0.02	0.03	0.08	0.02	0.04	
P <sub>2</sub> O <sub>5</sub>	0.01	0.00	0.00	0.00	0.01	0.00	0.00	0.01	0.00	0.00	0.00	0.00	0.00	0.02	0.02	0.01		
Total	101.26	100.35	100.12	97.51	88.38	101.33	99.55	98.45	100.20	100.32	99.33	94.63	99.86	98.75	98.03	98.26	98.58	

Oxides wt (%)	A18	A19	A21	A23	A24	A25	A26	A27	A28	A29	A30	A31	J-L 1975	Lun-Alk	Lun-Mg	Lun-Fan	
SiO <sub>2</sub>	47.34	47.81	47.47	47.50	47.42	47.35	47.05	47.14	47.60	47.33	52.03	45.45	35.30	44.30	43.20		
Al <sub>2</sub> O <sub>3</sub>	22.97	23.61	28.42	26.34	28.41	26.61	27.37	28.61	25.69	26.21	28.00	14.12	32.04	1.30	29.06	37.00	
TiO <sub>2</sub>	0.53	0.52	0.57	0.55	0.58	0.53	0.57	0.58	0.53	0.51	0.50	0.15	0.80	0.05	0.05	0.02	
Fe <sub>2</sub> O <sub>3</sub>	7.24	6.15	3.89	5.20	3.96	5.51	4.08	5.20	5.58	4.89	3.88	3.58	2.26	10.88	2.29	0.10	
MnO	0.09	0.10	0.10	0.09	0.08	0.10	0.08	0.09	0.11	0.07	0.09	0.07	0.03	0.11	0.03	0.01	
MgO	4.31	2.40	0.42	0.88	0.60	2.62	0.64	0.95	2.34	1.37	1.03	0.35	1.60	51.40	8.29	0.04	
CaO	14.89	13.17	16.74	15.61	16.80	15.65	17.06	15.56	15.70	13.96	17.73	1.22	16.06	1.30	16.40	19.50	
Na <sub>2</sub> O	0.92	2.17	1.22	1.29	1.23	1.48	0.91	0.82	1.15	1.30	0.98	3.22	1.31	0.04	0.32	0.38	
K <sub>2</sub> O	0.02	0.03	0.03	0.09	0.01	0.02	0.08	0.07	0.02	0.07	0.01	3.58	0.02	0.02	0.04	0.01	
P <sub>2</sub> O <sub>5</sub>	0.00	0.01	0.01	0.01	0.00	0.01	0.00	0.01	0.01	0.01	0.02	0.05					
Total	98.30	95.96	98.80	97.58	99.14	99.99	98.12	98.93	98.32	96.02	99.56	78.69	98.97	101.14	100.77	100.25	

**Table 3.1 Whole rock major oxides wt (%) of terrestrial and Lunar (alkaline, Mg-rich and Ferron) anorthosites**

Oxides wt (%)	A1	A2	A3	A4	A5	A6	A7	A8	A9	A10	A11	A12	A13	A14	A15	A16	A17
SiO <sub>2</sub>	47.70	47.85	47.80	47.54	50.22	47.95	47.60	47.81	47.76	47.71	47.69	47.27	47.66	46.40	48.93	47.20	47.54
Al <sub>2</sub> O <sub>3</sub>	27.11	29.71	27.26	27.08	22.39	28.42	24.80	25.19	23.35	22.98	27.17	24.36	25.69	24.55	25.27	20.60	25.20
TiO <sub>2</sub>	0.58	0.50	0.52	0.51	0.50	0.52	0.54	0.54	0.54	0.54	0.56	0.51	0.52	0.10	0.11	0.13	0.53
Fe <sub>2</sub> O <sub>3</sub>	6.49	3.21	4.71	3.88	2.97	4.44	6.40	5.26	7.49	7.92	5.56	4.03	5.44	4.10	2.58	4.91	6.27
MnO	0.09	0.05	0.07	0.05	0.04	0.06	0.08	0.07	0.10	0.10	0.07	0.06	0.07	0.05	0.04	0.07	0.14
MgO	2.49	0.93	2.65	1.29	0.31	2.31	3.94	3.42	4.94	5.52	2.08	2.29	3.85	7.35	4.24	9.53	2.84
CaO	15.44	16.71	15.81	15.86	7.13	16.22	14.86	14.95	14.79	14.35	14.86	14.97	15.40	14.63	15.35	14.47	14.61
Na <sub>2</sub> O	1.34	1.38	1.29	1.28	2.83	1.39	1.29	1.17	1.22	1.18	1.33	1.14	1.19	1.52	1.40	1.31	1.40
K <sub>2</sub> O	0.03	0.01	0.02	0.02	1.98	0.02	0.03	0.04	0.02	0.02	0.01	0.00	0.02	0.03	0.08	0.02	0.04
P <sub>2</sub> O <sub>5</sub>	0.01	0.00	0.00	0.00	0.01	0.00	0.00	0.01	0.00	0.00	0.00	0.00	0.00	0.02	0.03	0.02	0.01
Total	101.26	100.35	100.12	97.51	88.38	101.33	99.55	98.45	100.20	100.32	99.33	94.63	99.86	98.75	98.03	98.26	98.58

Oxides wt (%)	A18	A19	A21	A23	A24	A25	A26	A27	A28	A29	A30	A31	J-L 1975	Lun-Alk	Lun-Mg	Lun-Fan
SiO <sub>2</sub>	47.34	47.81	47.47	47.49	47.50	47.42	47.35	47.05	47.14	47.60	47.33	52.03	45.45	35.30	44.30	43.20
Al <sub>2</sub> O <sub>3</sub>	22.97	23.61	28.42	26.34	28.41	26.61	27.37	28.61	25.69	26.21	28.00	14.12	32.04	1.30	29.06	37.00
TiO <sub>2</sub>	0.53	0.52	0.57	0.55	0.58	0.53	0.57	0.58	0.53	0.51	0.50	0.15	0.80	0.05	0.05	0.02
Fe <sub>2</sub> O <sub>3</sub>	6.15	3.89	5.20	3.96	5.51	4.08	5.20	5.58	4.89	3.88	3.58	2.26	10.88	2.29	0.10	
MnO	0.09	0.10	0.09	0.08	0.10	0.08	0.09	0.11	0.07	0.09	0.07	0.03	0.11	0.03	0.01	
MgO	4.31	2.40	0.42	0.88	0.60	2.62	0.64	0.95	2.34	1.37	1.03	0.35	1.60	51.40	8.29	0.04
CaO	14.89	13.17	16.74	15.61	16.80	15.65	17.06	15.56	15.70	13.96	17.73	1.22	16.06	1.30	16.40	19.50
Na <sub>2</sub> O	0.92	2.17	1.22	1.29	1.23	1.48	0.91	0.82	1.15	1.30	0.98	3.22	1.31	0.04	0.32	0.38
K <sub>2</sub> O	0.02	0.03	0.03	0.09	0.01	0.02	0.08	0.07	0.02	0.07	0.01	3.58	0.02	0.02	0.04	0.01
P <sub>2</sub> O <sub>5</sub>	0.00	0.01	0.01	0.01	0.00	0.01	0.00	0.01	0.01	0.01	0.01	0.02	0.05			
Total	98.30	95.96	98.80	97.58	99.14	99.99	98.12	98.93	98.32	96.02	99.56	78.69	98.97	101.14	100.77	100.25

**Table 3.2 Major oxides (wt%) of terrestrial and lunar Gabbroic anorthosite rocks**

Oxides wt (%)	Sittampundi								Prakasam province (AP)			Lun	
	GA1	GA2	GA3	GA4	GA5	GA6	GA7	GA8	GA9	GA10	GA1	GA2	
SiO <sub>2</sub>	47.72	47.82	47.59	47.55	47.54	47.41	47.95	47.23	47.27	47.20	46.90	48.11	47.48
Al <sub>2</sub> O <sub>3</sub>	23.69	24.02	27.77	22.73	26.76	27.30	11.26	26.76	26.74	20.60	11.12	13.14	23.09
TiO <sub>2</sub>	0.53	0.53	0.52	0.53	0.57	0.60	1.34	0.55	0.57	0.13	0.68	1.09	0.74
Fe <sub>2</sub> O <sub>3</sub>	7.34	6.78	3.62	6.92	5.09	5.19	19.10	4.89	5.17	4.91	11.95	14.98	5.79
MnO	0.09	0.09	0.07	0.11	0.10	0.09	0.26	0.10	0.10	0.07	0.14	0.19	0.06
MgO	6.04	5.46	1.04	5.54	1.03	1.29	5.61	0.88	0.96	9.53	6.10	8.95	2.68
CaO	14.44	14.36	16.58	14.45	15.92	16.84	8.64	16.51	15.82	14.47	10.31	9.98	10.45
Na <sub>2</sub> O	1.21	1.42	1.30	0.92	1.31	1.15	1.52	0.88	1.10	1.31	1.09	1.63	2.82
K <sub>2</sub> O	0.05	0.03	0.02	0.02	0.06	0.03	1.45	0.04	0.02	0.02	0.28	0.48	0.67
P <sub>2</sub> O <sub>5</sub>	0.01	0.00	0.00	0.01	0.01	0.12	0.01	0.01	0.02	0.04	0.21	0.03	0.02
Total	101.12	100.52	98.50	98.76	98.38	99.89	97.25	97.86	97.76	98.26	88.61	98.75	94.62
											96.69	96.69	101.22

### Alkali-lime index diagram

Frost et al (2001) defined the modified alkali-lime index (MALI) from a plot of  $\text{Na}_2\text{O} + \text{K}_2\text{O}$  -  $\text{CaO}$  vs.  $\text{SiO}_2$ . They plotted compositions from the Peninsular Ranges batholith, Tuolumne intrusive suite, the Sherman batholith, and Bjerkeim-Sokndal intrusion on this diagram and used them to draw boundaries between calcic, calc-alkalic, alkali-calcic, and alkalic series. Each boundary is constrained to go through  $\text{MALI}=0$  at the value defined by Peacock (1934) (namely, alkalic – alkali-calcic at  $\text{SiO}_2=51.0$ , alkali-calcic - calc-alkalic at  $\text{SiO}_2=56.0$ , and calc-alkalic - calcic at  $\text{SiO}_2=61.0$ ). From these

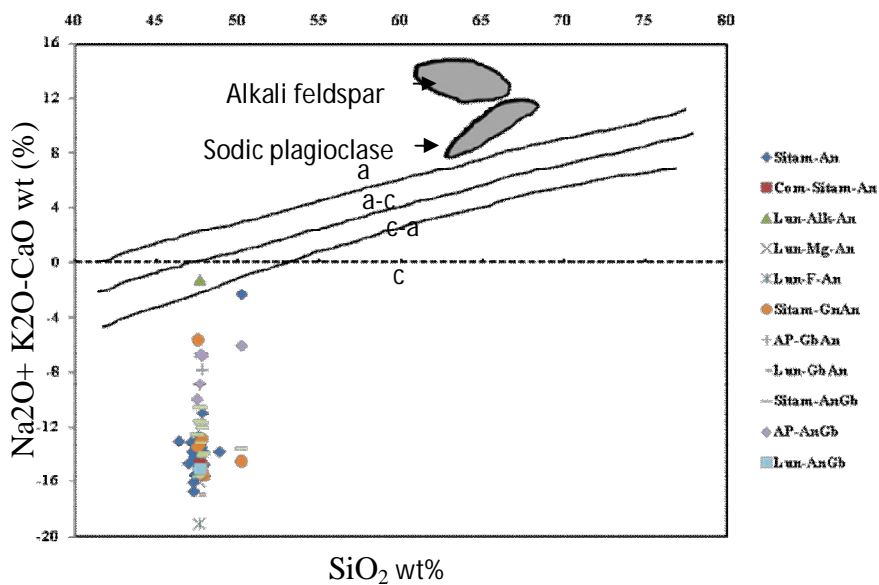


**Figure 3.12 Alkali-lime index (after Frost et al 2001)**

constraints, the boundaries were drawn by eye to separate as much as possible the individual suites (Frost and Frost 2008).

Further from Plot of the modified alkali-lime index,  $\text{Na}_2\text{O} + \text{K}_2\text{O}$ - $\text{CaO}$  (Frost et al 2001), against  $\text{SiO}_2$  (Figure 3.12) it may be observed that the lunar and terrestrial anorthosites are calcic rich.

The predominant plagioclase compositions among anorthositic rocks are revealed on plots of Na<sub>2</sub>O-CaO-(MgO+Fe) (Figure 3.12) which illustrate the high Ca content of plagioclase in Sittampundi. Molecular proportion of Al<sub>2</sub>O<sub>3</sub> exceeds the sum of Na<sub>2</sub>O and K<sub>2</sub>O, but is less than the sum of Na<sub>2</sub>O, K<sub>2</sub>O and CaO. These rocks tend to be rich in anorthite and usually also contain hornblende, epidote, biotite and pyroxene.

### **ACF and AFM diagrams**

Some workers (Barton et al 1979; Leelanandam and Narsimha Reddy 1985) have discussed major element compositional variations in Archean anorthosite complexes in terms of fraction trends and liquid lines of descent. However, the AFM diagram (Figure 3.13a) a useful discriminator of magmatic affinities and fractional trends for volcanic rocks should not be used in this regard for dominantly cumulate rocks found in Archean anorthosite complexes (Myers 1975b; Barton et al 1979). Such diagrams can be useful for example, to indicate the relatively primitive which have mg\* values (molar Mg/(Mg+Fe) up to 0.7 and therefore can be reliably interpreted as cumulate of early crystallizing mafic silicates. However, in this study ACF diagram has been considered. This is similar to the composition obtained by Ashwal (1993) for Sittampundi anorthosites. The Sittampundi complex anorthosites show calc-alkaline trends (Janardhanan and Leake 1975).

The trends in whole-rock chemistry among the dominant lithologies in Archean anorthosite complexes can be interpreted as cumulate mixtures of plagioclase and mafic silicates, possibly with small components of trapped liquid. This is particularly evident from the ACF diagram (Figure 3.13b), which further show that orthopyroxene and /or olivine dominate over clinopyroxene in the cumulate mafic silicate assemblages (Ashwal 1993).

Mineral phases plagioclase (Pl), clinopyroxene (Cpx), orthopyroxene (Opx), amphibole (Amp) and oxide are also plotted in this diagram. The arrow indicates the Fe enrichment of rocks from Panzhihua in comparison with the normal gabbros, which should follow the line between plagioclase and clinopyroxene. On a  $\text{MgO}-(\text{Al}_2\text{O}_3 + \text{CaO})-(\text{FeO}_{\text{total}} + \text{TiO}_2)$  diagram, all of the terrestrial rocks are richer in Fe and Ti, but poorer in MgO than normal gabbroic rocks (Figure 3.13c).

There are three distinct suits of plutonic rocks of the lunar surface they are, the Magnesium suite, the Alkali suite and a variety of evolved lithologies.

The Magnesian suite can be further divided into the olivine-bearing magnesian troctolite association (which includes troctolite, anorthosite, dunite and pyroxene – bearing troctolite) and the less abundant magnesian nortite association (includes norite, olivine norites, gabbronorites and ilmenite gabbros/norites).

Ferron anorthosite (FAN), which dominate highland suites in some eastern provinces (Apollo 15, Apollo 16) are rare in the Western Highland province (Heiken et al 1991).

The evolved lithologies include various types of rocks such as the KREEP, granite which is not included for this study.

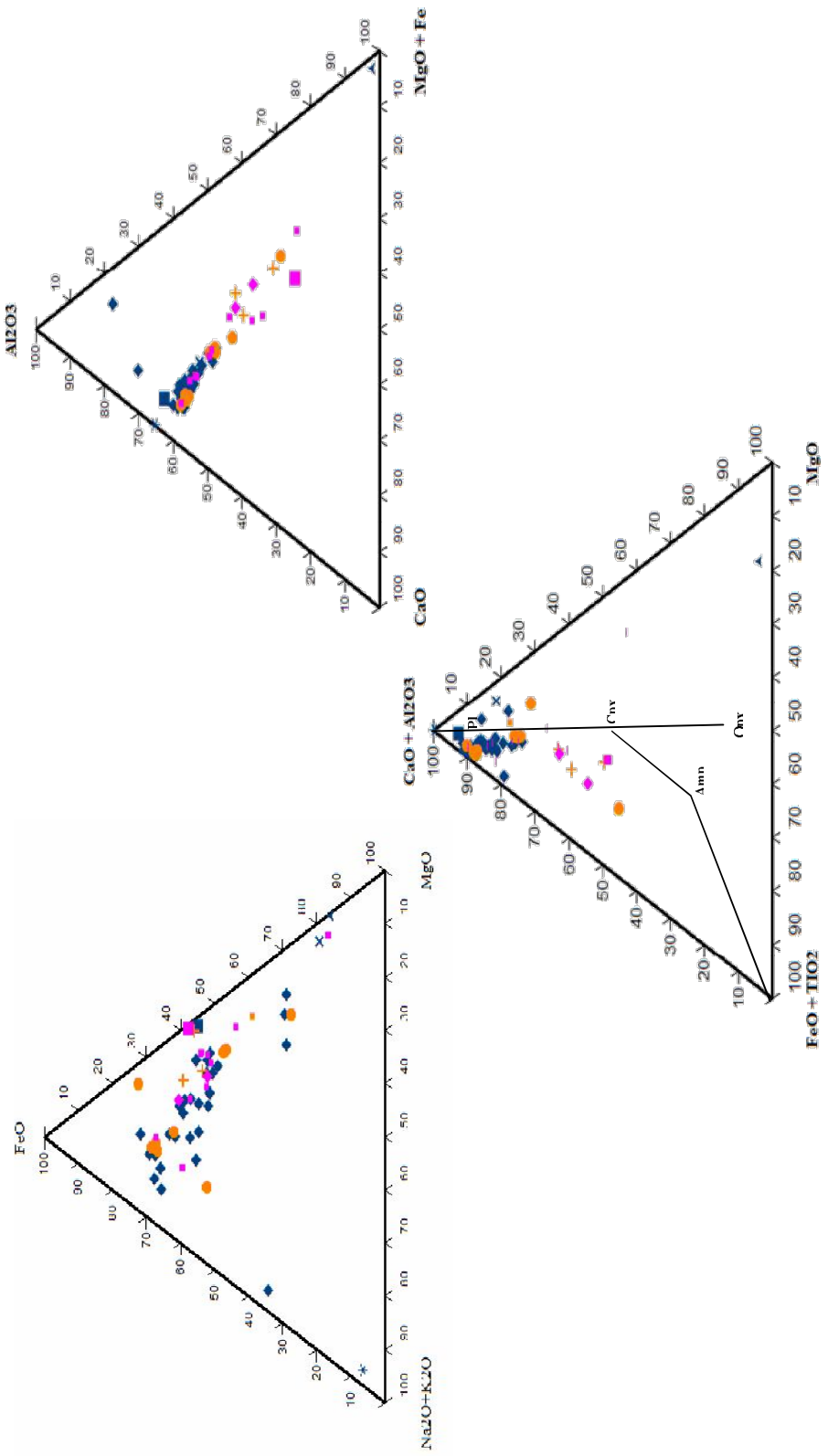


Figure 3.13 (a) AFM (b) ACF and (c) FeO +TiO<sub>2</sub>, CaO+Al<sub>2</sub>O<sub>3</sub>, MgO

Magnesian anorthosites are relatively new additions to the Mg-rich suite. These rocks are characterized by plagioclase-rich modes (90-99% plagioclase) with mineral composition with olivine (10-15%).

The alkali suite was first recognized by Warren and Wasson and subsequent studies established it as the second most common highland rock association at the Apollo 14 site. The most common lithologies are anorthosites and norite or gabbronorite; olivine norites are rare. The alkaline anorthosites are characterized by mode of 95-100% plagioclase with minor pigeonite, augite, K-feldspar, ilmenite, silica, whitlockite and Fe-metal.

The alkali suite represents cumulate rocks which crystallized from a KREEP parent magma. This magma was assimilated by Mg-suite parent magmas before they crystallized, or penetrated already crystallized Mg-suite plutons to enrich them metasomatically. It is not clear if the alkali suite cumulate rocks are consistent with this origin, but it does offer an attractive explanation to the contrasts in major elements compositions observed between the two suites.

### **3.7.3 Ultramafic Rock**

#### **3.7.3.1 Lunar dunite**

The lunar dunite may represent a cumulate formed during early differentiation (Laul and Schmitt 1973) of the moon. Dunite samples were recovered from samples 72415 to 72418 of Apollo 17 landing site (Ryder 1992). The dunite sample no. 72415 (Figure 3.14a) is made up of 93% olivine ( $\text{Fo}_{86-89}$ ), 4 % plagioclase, 3% pyroxene and the age was determined as very old 4,55 by (Meyer 2004). The olivines have shock features and plagioclase has been converted to maskelynite. Most of the plagioclase was crystalline laths (Dymek et al 1975). There are two types of proxenes, orthopyroxene and

augite (Dymek et al 1975). While the terrestrial deep plutonic olivines are zoned only at their extreme outer rims or where they are in subsolidus reaction with chromite. Olivines in volcanic rocks from both the earth and the moon have a wide range of compositions represented by zoning. The 72415 olivines are far too short for a deep plutonic origin (Ryder 1992). The texture of the dunite is metamorphic and resembles the tabular texture of terrestrial ultramafic xenoliths in basalt (Mercier 1972) in which olivine prisms are scattered sparsely in a granoblastic- polygonal matrix.

This dunite is comprised of angular to sub-rounded clasts (~60%) of pale-green to yellow olivine (up to 1 cm) set in a fine-grained, granulated matrix of mostly olivine. This cataclastic texture apparently resulted from simple crushing, without substantial recrystallization. Other minerals include pyroxene and plagioclase with minor troilite, iron grains, Cr-spinel, whitlockite and armalcolite reported (Dymek et al 1975; Meyer 2004).

### **3.7.3.2 Chalk hills dunite**

To study the dunite analogue samples from Chalk hills, Tamil Nadu were collected. The dunite rocks can be identified by hand specimen, it is bright olive green colour, vitreous lustre, and heavy. Thirty two dunite samples were selected for this study such a way that they are not serpentinised, or contain magnesite veins. Thin section (Figure 3.14b) show that the rock is almost entirely composed of olivine (95%) mineral with very few pyroxene (2-3%) and one or two grains of plagioclase feldspar (<1%) and few iron oxides. They are un-serpentized and occur as subhedral grains with suture boundary exhibiting granulitic texture.

To understand the lithological evolution of the dunite and to identify the analogue of the lunar geochemical analysis was carried out.

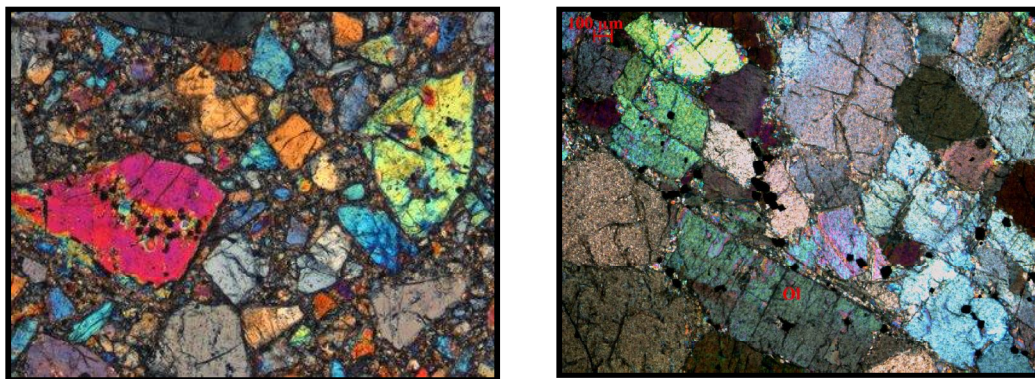


**Figure 3.14 Photomicrograph of (a) Lunar Dunite (sample no 72415)**  
**(Source : LPI atlas) (b) Dunite of Chalk hills**

### 3.7.3.3 Chemical correlation between the earth and moon dunites

To understand the lithological evolution of the dunite and to identify the analogue of the lunar geochemical analysis was carried out. Table 3.4 provides the 32 dunite samples from Chalk hills with 1 lunar dunite sample.

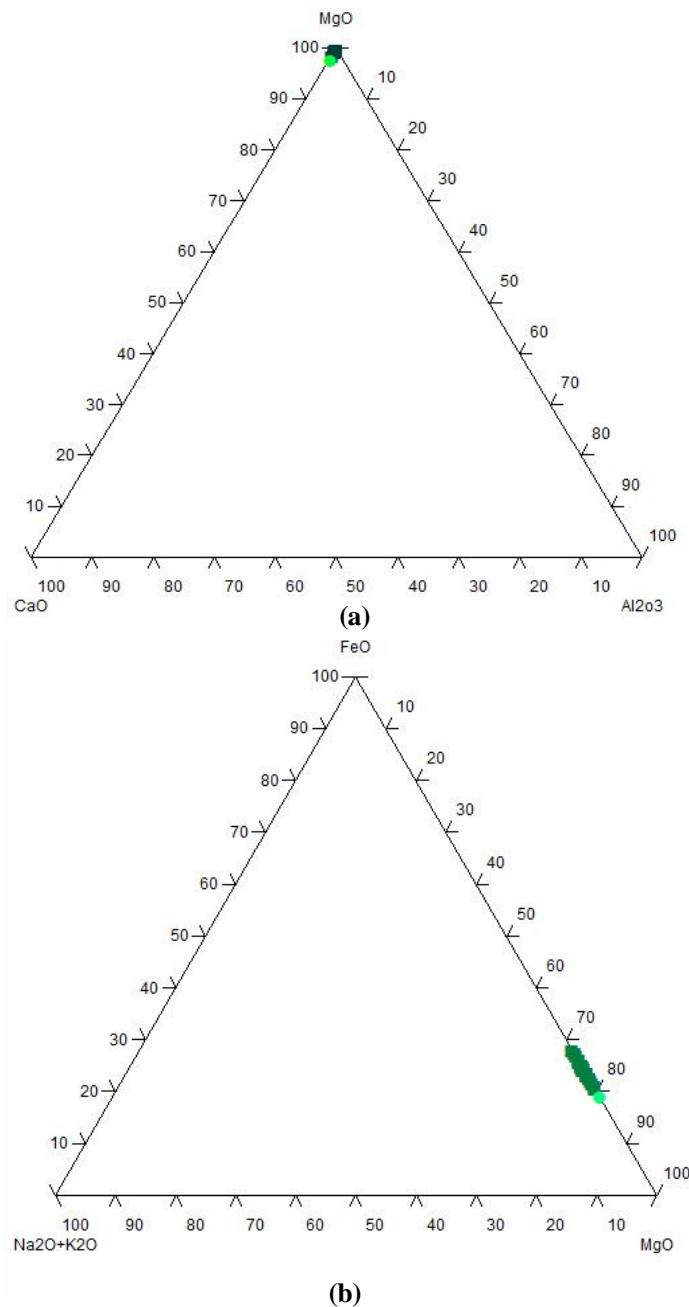
The AFM and MgO-CaO-Al<sub>2</sub>O<sub>3</sub> (Figures 3.13a,b respectively) of terrestrial and lunar dunites are rich in MgO content and fraction trend is ultramafic.

**Table 3.4 Major oxides (wt%) of Chalk hills dunite and Lunar dunite (sample no. 72415)**

Major oxides (%)	D1	D2	D3	D4	D5	D6	D7	D8	D9	D10	D11	D12	D13	D14	D15	D16
SiO <sub>2</sub>	37.16	37.21	37.71	37.54	38.47	37.02	36.49	36.73	37.42	37.26	36.80	36.95	37.67	39.01	36.63	38.38
Al <sub>2</sub> O <sub>3</sub>	0.83	0.29	0.23	0.47	0.29	0.32	0.40	0.25	0.38	0.30	0.58	0.31	0.29	0.61	0.30	0.32
TiO <sub>2</sub>	0.02	0.01	0.01	0.01	0.01	0.01	0.02	0.01	0.01	0.02	0.01	0.02	0.01	0.02	0.01	0.02
Fe <sub>2</sub> O <sub>3</sub>	15.38	14.61	14.74	16.40	14.50	15.69	15.37	17.14	16.42	16.09	15.28	17.64	12.88	12.98	15.62	14.88
MnO	0.20	0.18	0.20	0.25	0.23	0.22	0.25	0.26	0.22	0.24	0.23	0.24	0.22	0.21	0.21	0.22
MgO	41.95	43.05	44.17	41.77	45.07	42.60	42.29	41.81	42.09	43.07	41.09	40.85	43.63	45.43	41.70	43.56
CaO	0.43	0.36	0.28	0.38	0.48	0.28	0.26	0.29	0.35	0.28	0.35	0.35	0.32	0.26	0.23	0.20
Na <sub>2</sub> O	0.11	0.01	0.13	0.08	0.03	0.03	0.04	0.04	0.07	0.05	0.08	0.06	0.01	0.06	0.04	0.05
K <sub>2</sub> O	0.02	0.01	0.01	0.01	0.02	0.01	0.02	0.03	0.04	0.02	0.03	0.03	0.02	0.02	0.03	0.03
P <sub>2</sub> O <sub>5</sub>	0.01	0.01	0.01	0.01	0.01	0.01	0.01	0.01	0.02	0.01	0.01	0.01	0.01	0.01	0.01	0.01
Total	96.10	95.75	97.48	96.93	99.11	96.19	95.15	96.57	97.02	97.34	94.46	96.45	95.06	98.61	94.77	97.66

Major oxide (%)	D17	D18	D19	D20	D21	D22	D23	D24	D25	D26	D27	D28	D29	D30	D31	D32	LUN
SiO <sub>2</sub>	38.05	36.26	37.23	37.13	36.25	36.69	36.74	37.48	36.94	37.37	36.52	36.26	36.77	37.84	37.38	37.73	40.60
Al <sub>2</sub> O <sub>3</sub>	0.55	0.31	0.59	0.46	0.38	0.29	0.23	0.32	0.25	0.25	0.61	0.36	0.33	0.39	0.41	0.19	1.20
TiO <sub>2</sub>	0.01	0.01	0.02	0.01	0.02	0.01	0.01	0.01	0.01	0.01	0.06	0.02	0.01	0.02	0.01	0.01	0.03
Fe <sub>2</sub> O <sub>3</sub>	15.12	16.92	15.08	14.68	15.63	14.12	14.85	13.65	13.68	15.66	16.73	15.01	13.66	13.28	14.22	14.91	11.90
MnO	0.24	0.24	0.24	0.21	0.23	0.21	0.23	0.22	0.20	0.28	0.25	0.26	0.24	0.22	0.23	0.19	0.11
MgO	42.08	40.47	41.70	41.38	40.44	42.08	41.65	43.67	42.51	42.77	39.95	41.40	42.20	43.68	42.59	43.54	45.40
CaO	0.27	0.23	0.28	0.36	0.33	0.32	0.23	0.29	0.24	0.25	0.70	0.35	0.29	0.40	0.32	0.22	1.10
Na <sub>2</sub> O	0.10	0.04	0.12	0.06	0.14	0.02	0.04	0.02	0.01	0.09	0.03	0.06	0.07	0.05	0.05	0.01	
K <sub>2</sub> O	0.05	0.03	0.06	0.08	0.04	0.02	0.02	0.02	0.01	0.01	0.03	0.04	0.03	0.03	0.01	0.00	
P <sub>2</sub> O <sub>5</sub>	0.01	0.01	0.01	0.01	0.01	0.01	0.01	0.01	0.01	0.01	0.01	0.01	0.01	0.01	0.01	0.01	
Total	96.48	94.52	95.32	94.38	93.46	93.76	94.01	95.68	93.88	96.62	94.96	93.73	93.60	95.94	95.25	96.84	100.36



**Figure 3.15 (a) AFM diagram (b)MgO-CaO-Al<sub>2</sub>O<sub>3</sub> of Dunites**

### 3.7.4 Ultrabasic Rock

#### 3.7.4.1 Lunar basalt

Mare basalts are classified using several properties, including chemical composition, remanent magnetism, radioactivity, mineralogy, texture, and age (Soderblom et al 1977; Boyce 1976: Boyce and Johnson 1977). The chemical parameters commonly used to subdivide basalts are  $\text{TiO}_2$ ,  $\text{Al}_2\text{O}_3$ ,  $\text{MgO}$ ,  $\text{K}_2\text{O}$ , and the rare earth elements (REE). Titanium dioxide is especially useful as it exhibits the largest range of values and provides a method of classification that is discernible using both chemical and remote sensing methods. Lunar sample workers commonly divided mare basalts into two main groups : low-Ti and high-Ti (Taylor et al 1991). The remaining classifications used include very low as a commonly used designation for values  $<1.0$  wt%  $\text{TiO}_2$ , low for range of 1.0-4.5 wt%  $\text{TiO}_2$ , high for the range 7.5-10.0 wt%  $\text{TiO}_2$ , and very high for values  $>10.0$  wt%  $\text{TiO}_2$  (Giguere et al 2000).

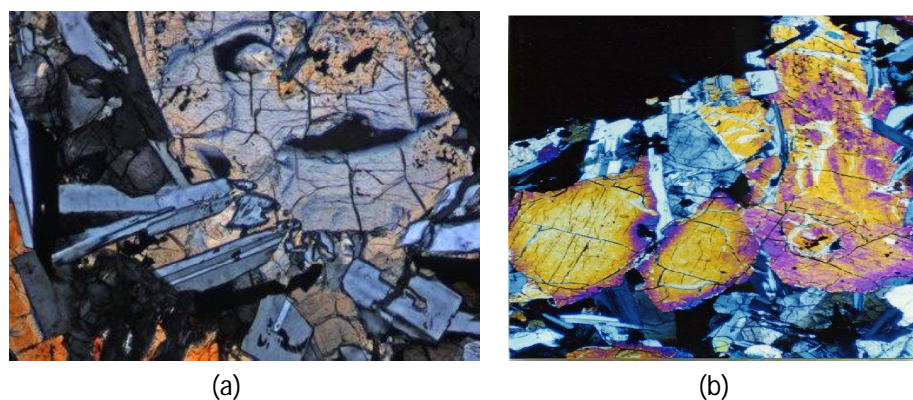


**Figure 3.16 Lunar basalt (a) subophitic -12017 (b) vesicular- 15016**  
**(Source : Lunar atlas-LPI)**

To study the analogue basalt rock, the lunar basalt sample 12017 (compact type) and sample 15016 were chosen as the composition was similar to that of the Deccan basalts. Baldridge et al (1979) describe 12017 (Figure 3.16a) as a porphyritic rock with a medium-grained, variolitic to subophitic

groundmass. Plagioclase width is ~190 microns. It is composed of plagiocalse (25%), olivine (5%), pyroxene (61%), ilmenite (1.5%) given by Neal et al (1994).

Lunar sample 15016 is a medium-grained basalt with subhedral phenocrysts of zoned pyroxene (1-2 mm) and olivine (~1 mm) set in a matrix of subophitic intergrowths of pyroxene and plagioclase (Figure3.16b). Vesicles (1 to 5 mm) make up about 50 % of the volume. Opaque minerals (ilmenite and ulvöspinel) frequently border the vesicles. Plagioclase platelets are sometimes hollow, with pyroxene cores. Subrounded grains of Cr-spinel are found in the pyroxene and olivine phenocrysts. Troilite and Fe-Ni metal are found in the mesostasis. Large pyroxene grains are highly zoned first towards Ca-rich, then Fe-rich, indicating rapid crystallization (Bence and Papike (1972), Papike et al (1976), and Kushiro (1973)).

### **3.7.4.2 Lonar Basalt**

The Lonar basalt rocks are mostly weathered, megascopically they appear as light (moderately weathered) to dark grey (less weathered) in colour. The cooling was so fast that no visible crystals were formed (aphenitic). There are few vesicles (due to escape of volatiles) forming the vesicular basalt and sometimes they are filled with amygdalyes (calcite or zeolites) and form the amygdaloidal basalt. Thus the Lonar basalts contain three types of basalts (compact, vesicular and amygdoloidal basalts).

To know the mineralogy, thin sections were prepared and they show that the rock is composed of predominantly of 40-45% plagioclase (labradorite), 30-35% pyroxene (augite and pigeonite) and 20-25% olivine and <10% rest iron oxides (illmenite and magnetite). The absence of quartz means that it is difficult to classify the shock level in these basalts, particularly at low to moderate shock levels (i.e., ~2–20 GPa), where shock-

produced glasses are absent or rare. Pioneering studies of the shock petrography of the Lonar Crater basalts were conducted by Schaal (1975) and Kieffer et al (1976). These workers noted that the main shock effects are the conversion of plagioclase to diaplectic glass (Nayak 1993) and vesiculated feldspar glass, and undulatory extinction in pyroxene. Shock effects on the paleomagnetism of Lonar Crater are subtle and consistent with low to moderate shock level (Cisowski et al 1977; Rao and Bhalla 1984; Louzada et al 2008).

The most important constituent minerals in the basalt samples studied are the plagioclases are euhedral, pyroxene forms the ground mass along with iron oxides and glass. Olivine grains of irregular shape are present in the ground mass. This is typical of sub-ophitic texture (laths of plagioclase on augite groundmass) is shown in the compact basalts (Figure 3.17a).

The magma composition and its cooling history are reflected by the textures and mineralogical assemblages. The grain sizes are variable (phyric to aphyric) and crystallinity ranges between holohyaline and holocrystalline. The presence of highly embayed phenocrysts in disequilibrium with the host magma supports the importance of magma mixing in the evolution of the Deccan basalts (ref). The plagioclases are phenocrysts always occur as glomerocrysts and generally have corroded margins in contact with groundmass. The commonly observed phenocryst assemblages in Deccan basalts are: plagioclase + olivine + augite (Figure 3.17b). Augite phenocrysts are scarce and usually occur with abundant olivine and plagioclase. Olivine and calcic plagioclase crystallize first followed by augite and Fe–Ti oxides. Olivine is usually euhedral but more anhedral in pyroxene-rich rocks. Clinopyroxene phenocrysts are colourless to pale green augite.

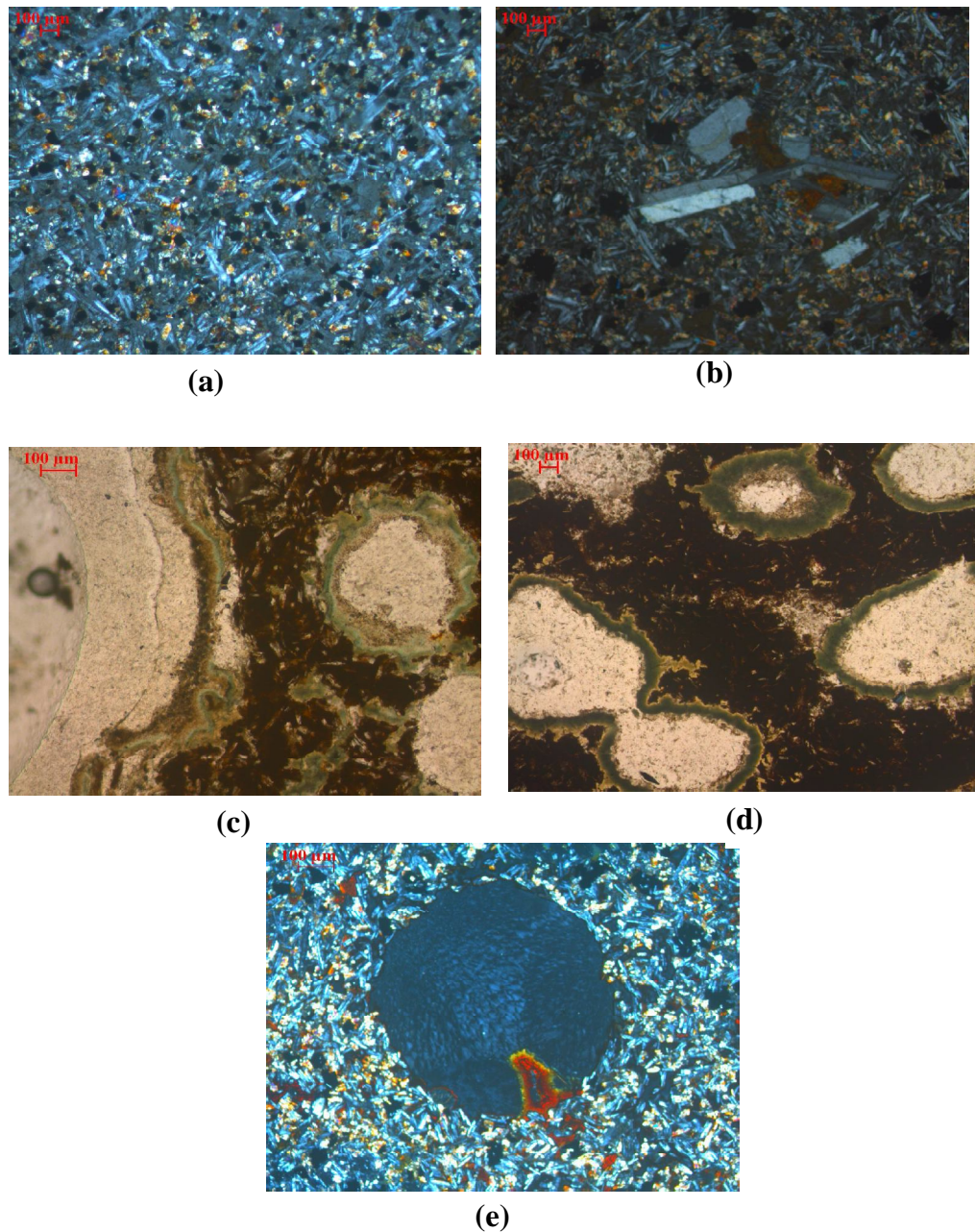


**Figure 3.17** Thin section photographs of Lonar basalts (a) Compact (b) basalt with plagioclase phenocryst (c) vesicular basalt (d) amygdyloidal basalt (e) basalt with spherule

The compact basalts are generally medium-fine grained plagioclase feldspars, augite are common minerals, in few samples glassy matrix is observed due to rapid cooling, in many samples large laths of plagioclase feldspar are present (Figure 3.17b) these minerals would have been a part of the magma itself or they are mixed during the lava flow is not known. The vesicular basalt (Figure 3.17c) show laths of plagioclase feldspar with pyroxene ground mass, with many vesicles. While the secondary mineral calcite and zoisite are present in few samples forms the amygdoloidal basalt (Figure 3.17d) type. Few samples show glass spherules (Figure 3.17e) like form may be formed during the meteoritic impact.

### **3.7.4.3 Chemical correlation between the earth and moon basalts**

To identify the parental magma of the basalts geochemical analysis carried out for the Lonar samples include 34 basalt samples, 4 ejecta, 2 soil and 1 basalt powder (mare stimulant). Kennedy (1933) pointed out that there exists two different kinds of parental basaltic magmas which show contrasting differentiation trends regardless of the conditions of crystallization: one is toward saturation and oversaturation with  $\text{SiO}_2$  (i.e. a nonalkalic trend), whereas the other is toward an increasing degree of undersaturation with  $\text{SiO}_2$  (i.e. an alkalic trend). The nonalkalic (subalkalic) trends are further classified into (i) calc-alkalic series (CA-Bowen trend) and (ii) tholeiitic series (TH-Fenner trend).

For this study the major oxides like  $\text{SiO}_2$ ,  $\text{Al}_2\text{O}_3$ ,  $\text{Fe}_2\text{O}_3$ ,  $\text{MnO}$ ,  $\text{MgO}$ ,  $\text{CaO}$ ,  $\text{Na}_2\text{O}$ ,  $\text{K}_2\text{O}$ ,  $\text{TiO}_2$ ,  $\text{P}_2\text{O}_5$  were quantified using X-ray fluorescence technique at Physical Research Laboratory, Ahmedabad, India. Apart, geochemical data were also compared with published (Lon-Com-Bas) Osae et al (2005) and with lunar mare basalt (Table 3.5). The geochemical analysis includes Silica-alkali, alkaline vs. subalkaline, AFM diagrams and Harker bivariant diagrams.

### **Alkali-silica analysis**

Figure 3.18a showing the Hawker variation diagram of wt%  $\text{Na}_2\text{O} + \text{K}_2\text{O}$  versus wt. %  $\text{SiO}_2$  provides a useful way of displaying the wide compositional range of terrestrial volcanic rocks and their nomenclature. This diagram is based on that of Cox et al (1979), and is consistent with the IUGS systematic classification of igneous rocks (Le Bas et al 1986). A simple diagram like this is preferable in the classification of igneous rocks as it makes direct use of their major element chemical composition, expressed in terms of wt. % constituent oxide.

Such diagram is only applicable to the classification of the commonly occurring non-potassic volcanic rocks and the nomenclature of their rarer potassic equivalents. Moreover, they are used only used to classify fresh unmetamorphosed volcanic rocks, as alkalis are mobile during weathering and metamorphism (Wilson 1989). In this diagram the volcanic rocks may be subdivided into members of two major magma series, alkali and sub-alkalic, separated by the solid line. Such division was first proposed by Iddings in 1982 and elaborated by Harker (1909), McDonald and Katsura (1964), Macdonald (1968), Irvine and Baragar (1971) and Miyashiro (1978). Each of these magma series contain rocks ranging from basic to acid in composition, and although the boundary between them is marked as a solid line it is actually gradational. Broadly speaking, the compositional range of volcanic rocks displayed in this diagram may be regarded as a consequence of two fundamental processes partial melting and fractional crystallization (Wilson 1989). Figure 3.18a, indicate that the Lonar samples belongs to basaltic (mostly) and few are basaltic-andesite types.  $\text{SiO}_2$  ranges between 46 and 51%. The Lunar basalt sample no. 12017,36 (Neal et al 1994) has 47%  $\text{SiO}_2$ .

### **Alkali Vs Subalkali**

If we compare rocks with the same  $\text{SiO}_2$  content, rocks of alkali series usually have higher  $\text{Na}_2+\text{K}_2\text{O}$  and lower  $\text{CaO}$  contents than those of

nonalkalic series. Thus, alkali and nonalkalic series may be distinguished with Harker-type variation diagrams (Figure 3.18b) with  $\text{SiO}_2$  on the abscissa (Harker 1909). This method was adopted particularly by Kuno (1959,1966) and Macdonald and Katsura (1964) demonstrated that the fields of alkali and tholeiitic rocks in Hawaii can approximately divided by a straight line in an  $\text{SiO}_2$  vs.  $\text{Na}_2\text{O} + \text{K}_2\text{O}$  diagram below. In this study (Figure 3.18b) it was observed that the Lonar basalts and the Lunar mare basalt (12017,36) belongs to Subalkali magma.

### **AFM diagram**

Wilson (1989); Wager and Deer (1939) demonstrated the usefulness of triangular diagrams with the AFM ( $A = \text{Na}_2\text{O}+\text{K}_2\text{O}$ ,  $F = \text{FeO}+\text{Fe}_2\text{O}_3$ ,  $M = \text{MgO}$ ) at the corners for distinguishing between tholeiitic and calc-alkaline differentiation trends in the sub-alkalic magma series. In such a diagram, the early and middle stages of crystallization of typical TH series are represented by curves approximately parallel to the  $\text{MgO}-\text{FeO}$  side, and in the late stage, a sharp turn occurs toward the  $\text{Na}_2\text{O}+\text{K}_2\text{O}$  corner to indicate more silicic rocks. On the other hand rocks of typical CA series show trends nearly perpendicular to the  $\text{MgO}+\text{FeO}$  side. A complete gradation exists between typical TH and typical CA series.

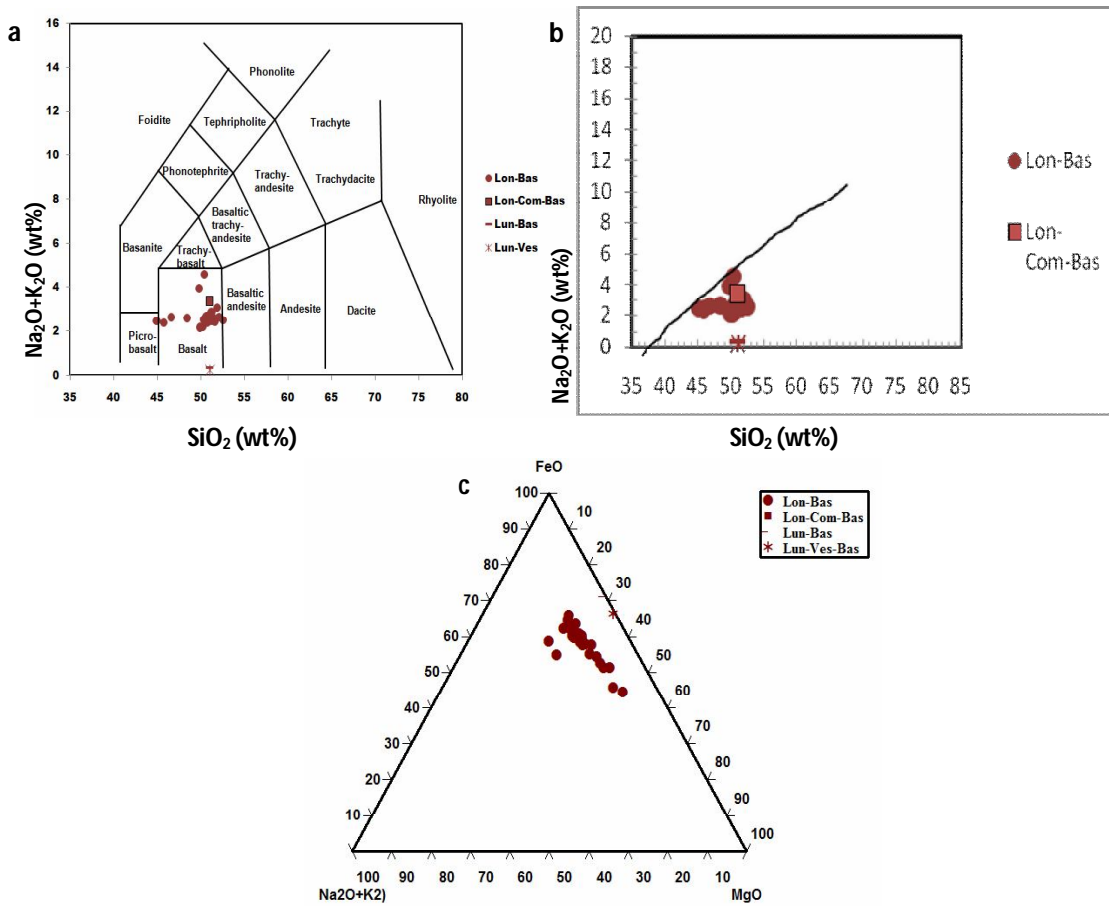
Two series can be differentiated in terms of their trends on an AFM diagram, in which tholeiitic suites commonly show a strong trend of iron enrichment in the early stages of differentiation, whereas calc-alkaline suites trend directly across the diagram, due to the suppression of iron enrichment by early crystallization of Fe-Ti oxides (Wilson 1989) shown in Figure 3.18c. The AFM diagram after Osae et al 2005 confirm the tholeiite type for the Lonar basalt and also the lunar mare basalt (12017,36,15016) also belongs to this type of magma.

**Table 3.5 Whole rock major oxides (wt%) of Lonar basalts and Lunar basalts**

Major oxides	B1	B2	B3	B4	B5	B6	B7	B8	B9	B10	B11	B12	B13	B14	B15	B16	B17	B18
SiO <sub>2</sub>	51.02	45.78	50.65	52.12	50.99	50.49	51.50	51.19	50.79	51.13	49.95	50.79	50.39	52.59	51.05	49.84	50.49	50.75
Al <sub>2</sub> O <sub>3</sub>	13.37	13.07	13.85	13.49	13.90	13.58	14.00	13.73	13.84	13.56	13.84	13.53	13.42	13.83	14.12	13.86	14.01	
Fe <sub>2</sub> O <sub>3</sub>	14.11	14.96	13.55	14.32	13.74	13.48	14.45	13.76	13.71	13.81	13.32	13.57	13.56	13.86	13.83	12.32	13.65	13.58
MnO	0.20	0.21	0.20	0.18	0.20	0.20	0.20	0.21	0.20	0.20	0.19	0.19	0.20	0.18	0.20	0.16	0.20	0.19
MgO	5.94	10.42	4.91	6.67	5.61	4.51	4.50	7.30	4.71	6.04	4.68	6.23	4.43	4.29	5.56	3.84	5.68	5.91
CaO	9.45	9.24	10.01	6.69	10.36	9.88	9.34	9.82	9.70	10.26	9.91	9.88	9.40	8.81	10.12	8.49	10.26	10.33
Na <sub>2</sub> O	1.96	2.04	2.17	1.15	2.28	2.08	2.21	2.10	2.16	2.20	1.86	2.17	2.00	2.13	2.17	2.00	2.13	2.20
K <sub>2</sub> O	0.49	0.34	0.49	1.49	0.45	0.47	0.38	0.65	0.46	0.57	0.30	0.53	0.50	0.37	0.29	1.94	0.37	0.37
TiO <sub>2</sub>	2.99	2.34	1.99	2.75	2.43	2.13	2.28	2.01	2.50	2.11	1.62	2.21	2.17	2.25	2.36	1.12	2.07	1.93
P <sub>2</sub> O <sub>5</sub>	0.40	0.26	0.39	0.15	0.35	0.38	0.26	0.26	0.36	0.28	0.32	0.36	0.30	0.25	0.33	0.56	0.30	0.30
Total	99.92	98.66	98.20	98.99	100.32	97.59	98.70	101.29	98.32	100.44	95.69	99.77	96.48	98.15	99.74	94.40	98.99	99.56

	B19	B20	B21	B22	B23	B24	B25	B26	B27	B28	B29	B30	B31	B32	B33	B34	Osae	Lunar	Lun-Ves
SiO <sub>2</sub>	50.99	51.26	50.82	51.27	51.93	46.65	51.02	44.97	51.22	50.23	51.64	50.47	50.70	51.15	50.81	48.45	47.82	47.27	43.97
Al <sub>2</sub> O <sub>3</sub>	13.94	13.93	14.03	14.10	13.97	14.05	13.90	13.47	14.00	13.74	13.46	13.60	14.14	13.87	13.87	12.82	12.96	10.00	8.43
Fe <sub>2</sub> O <sub>3</sub>	13.84	13.72	13.17	13.29	14.08	14.14	13.59	13.21	13.63	13.10	14.60	13.50	12.82	13.20	13.40	12.17	15.80	21.92	25.11
MnO	0.20	0.20	0.19	0.20	0.18	0.18	0.19	0.15	0.20	0.18	0.21	0.19	0.19	0.21	0.20	0.16	0.19	0.29	0.33
MgO	4.77	5.23	7.54	8.31	4.53	9.37	5.91	12.30	5.79	6.49	4.37	5.40	5.31	5.24	5.74	10.35	6.07	7.63	11.14
CaO	9.66	9.99	10.90	11.47	8.06	8.88	10.44	9.13	10.38	10.64	9.16	10.94	11.03	9.88	10.26	9.29	9.85	10.97	9.40
Na <sub>2</sub> O	2.14	2.32	2.11	2.22	2.09	2.19	2.05	2.26	1.90	2.20	2.83	2.09	2.49	2.15	2.21	3.00	0.27	0.21	
K <sub>2</sub> O	0.58	0.56	0.27	0.24	1.00	0.35	0.32	0.41	0.21	0.27	0.22	1.74	0.43	0.29	0.40	0.38	0.38	0.09	0.03
TiO <sub>2</sub>	2.29	2.37	1.97	2.25	2.28	2.08	2.32	1.72	2.23	2.86	1.28	2.18	1.94	2.39	2.26	3.37	2.31		
P <sub>2</sub> O <sub>5</sub>	0.38	0.32	0.24	0.23	0.23	0.25	0.36	0.24	0.38	0.22	0.28	0.33	0.21	0.34	0.26	0.27	0.09	0.07	
Total	98.79	99.88	101.22	103.57	98.35	98.38	100.20	98.01	100.37	98.49	98.37	101.86	98.18	98.85	99.12	98.48	98.60	101.90	101.00



**Figure 3.18** Hawker variation diagram of wt%  $\text{Na}_2\text{O} + \text{K}_2\text{O}$  versus wt%  $\text{SiO}_2$  b) Harker-type variation diagrams alkaline vs. subalkaline. C) AFM diagram

### 3.8 REGOLITHS

Meteorite impacts are a major geological force on the Moon. Most of the lunar surface is covered with fine-grained soil. Major bombardment by large asteroid-size bodies on the Moon ( $\sim 3.8$  billion years ago), the micrometeorite impacts been the major agents in modifying the upper few centimeters of the lunar regolith. Interplanetary micrometeorites consist of minute grains (mostly 10–150 m) that can be travelling at velocities well over

100,000 km/hr, imparting tremendous kinetic energy to the surfaces they hit. The major effect of larger impacts is the crushing and pulverizing of rocks and minerals (combination), thereby, decreasing their grain size (Anand et al 2004).

The moment that fresh bedrock is exposed on the Moon, meteoroid bombardment begins to destroy it. As the impacts continue, the original bedrock is covered by a fragmental layer of broken, melted and altered debris. This layer is called the lunar regoliths (Heiken et al 1991). The lunar science community has generally used the word soil in an engineering geology sense. Although lunar soil is lexicographically synonymous with lunar regolith (Bates and Jackson 1980), the lunar soil usually refers to the fine-grained fraction of the unconsolidated material (regolith) at the lunar surface (Heiken et al 1991).

The moon is covered with unconsolidated debris called the lunar regoliths. It is formed mostly by meteorite impact and space weathering (Chapter 1). It covers about 10 to 30 m thick over older highland regions and about 4 to 8 m thick over mare regions (Battler 2006). A typical sample of this regolith could be characterised as grey, poorly sorted pebble or cobble-bearing silty sand. The composition varies from basaltic to anorthositic (Mc Kay and Blaik 1991), and grain size varies from 1mm to <100 microns (Heiken et al 1991).

Lunar regolith is an unconsolidated material covering the entire surface of the Moon. It is about 4 to 8 m thick over the Mare regions, and roughly 10 to 30 m thick over the older Highland regions (Heiken et al 1991). More than 80% of the lunar bedrock is composed of the ANT suite rocks of the Highlands, with Mare basalts accounting for only ~17% of the bedrock. Lunar regolith is a complicated substance unlike any material found on the Earth, due, in part, to the lack of an atmosphere and atmospheric weathering

processes on the Moon. Regolith is composed of particles that were derived either from lunar bedrock, or from older regolith, which was formed when repeated meteoroid impacts pulverized the lunar bedrock, over-turning and mixing it, until it became a fine powder. Regolith is still undergoing modification and evolution today, and thus it is a dynamic material. It consists of mineral fragments, rock fragments, breccia fragments, glasses, and agglutinates (smaller particles, bonded by vesicular glass). Particles are heterogeneously mixed, and can range in size from microscopic to several meters or more in diameter.

There are no natural lunar regolith analogues on Earth, and supplies of existing lunar simulants are currently limited or running out, and may not be compositionally representative of typical lunar regolith. To date, all major lunar simulants produced have been based on basalt; however, the bulk of the lunar bedrock - including some potential landing sites, and likely much of the south pole region - is dominated by anorthosite-norite-troctolite (ANT) suite rocks. Therefore, it is particularly important to gain an understanding of the physical/mechanical behavior of anorthositic regolith (Battler et al 2006). To prepare for upcoming robotic Chandrayaan missions, equipment must be tested on the Earth using a good physical/mechanical stimulant. In this study apart from anorthosite simulant basalt regolith simulant was also carried out.

### **3.8.1      Regoliths and simulants**

The moon is stable but heavily cratered surface provides evidence that is continuously bombarded by external objects. Meteoritic impact is a major transport process on the lunar surface, because it redistributes materials both laterally and vertically, either by sedimentation from ballistic trajectories or by upward subsurface motion. Depending on the size of the event, impacts can pulverize surface boulders, shatter subsurface bedrock, or even dislodge crustal sections tens of kilometres deep. Impact is also the most important

metamorphic process on the moon, causing characteristic shock deformation, heating, melting, vaporization and even ionisation of pre-existing minerals and rocks (Heiken et al 1991).

Repetitive and frequent impacts agitate the lunar surface by shattering, burying, exhuming, tumbling and transporting individual grains in a random fashion. These processes gradually develop a fine-grained powdery layer on the lunar surface above the actual bedrock. This layer, called the regolith (Morris 1978). Regolith thicknesses >10 meters, may occur in highlands, thus the regoliths are prominent landforms on the lunar surface. Hence, in this study to understand the regoliths laboratory simulants were prepared and studies have been carried out.

Along with the pulverisation the materials of the lunar surface is also contaminated by meteoritic materials. There is no natural regolith analogues available on Earth (Battler 2006), hence in this study an attempt has been made to carry out the regolith stimulant study was made by natural (Lunar impact-ejecta and soil) and from crushing and pulverising sample (Chapter 1).

### **3.8.1.1 Comparison of Lunar Highland regoliths and simulant**

For the anorthosite regolith studies, a lunar anorthositic rich soil 67461,74 was compared with the laboratory derived simulant geochemistry.

The oldest anorthosite (Sittampundi Archean) was chosen for the simulant for regoliths, grain sizes 1003- 85 µm, 850- 600 µm, 600-420 µm, 420-210 µm, 210- 105 µm, 105 - 90 µm , 90-75µm, 75-63µm, 63-53µm, 53-45µm, 45-25µm fine - sizes were prepared (more detail in Chapter 2). Using XRF technique major oxides were determined and they were compared with the grain sizes of Apollo 15 highland regolith/soil samples 67461,74 (Table).

Since this study deals with the analogue rocks study to understand the effect of grain size on spectra, one of the Sittampundi anorthosite was chosen and pulverized to replicate the lunar anorthosite regoliths/soil and was compared with the lunar soil. The lunar soil 67461, 74 the purest highland soil composed of plagioclase (80%), pyroxene (9%), olivine (4%), highland glass (7%), Papki and White (1981) was chosen was compared.

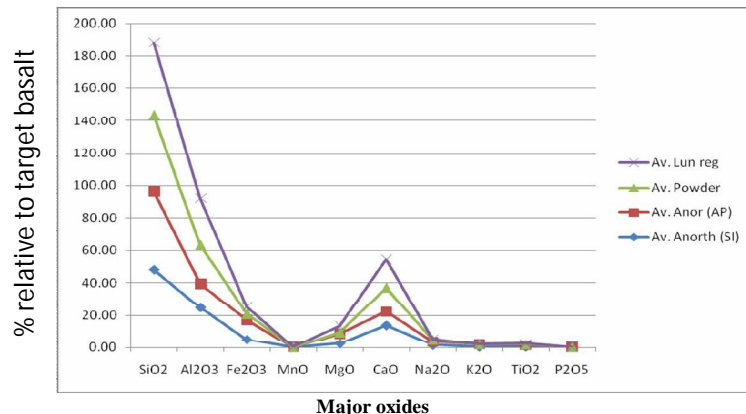
Within a given lunar soil, a similar scheme is apparent from larger to finer size fractions. With decrease in grain size, the abundances of the agglutinitic glasses increase. Although there is also a tendency for the plagioclase to slightly increase in the finer fractions, there are distinct decreases in pyroxene and olivine with decreasing grain size. Therefore, the ferromagnesian minerals decrease proportionately, while the plagioclase abundances stay constant or increase slightly.

The highland simulant rocks show similar trend of mineralogical show little variation from the natural highland lunar soil. As the grain size decreases the plagioclase remains almost constant while there is slight increase mafic concentration because the hornblende is present in the terrestrial sample and tends to pulverize than the pyroxene and plagioclase.

It may be observed from the Table 3.6 that the lunar regoliths are still finer than the simulants however, apart from the simulant the average bulk/massive rock geochemistry of the Sittampundi anorthosite were compared (Figure 3.19).

**Table 3.6 Major oxide wt (%) of lunar highland regolith and simulant**

	Size	Sio2	Tio2	Al2O3	FeO	MgO	Cao	MnO	Na2O	K2O	MnO
lunar	bulk	45	0.29	29.20	4.20	3.90	17.60	0.055	0.430	0.055	0.055
	>90	45.3	0.29	28.70	4.30	3.90	17.20	0.060	0.420	0.050	0.060
	20-90	44.4	0.40	28.80	4.50	4.60	17.20	0.062	0.430	0.055	0.062
	20-10 mic	44.3	0.40	29.30	4.40	4.00	17.60	0.065	0.420	0.062	0.065
	<10	45.1	0.29	28.60	4.30	4.30	16.50	0.060	0.430	0.070	0.060
	ave	44.82	0.33	28.92	4.34	4.14	17.22	0.060	0.426	0.058	0.060
Simulant	90-75 $\mu\text{m}$	47.273	0.502	25.983	3.233	0.941	15.337	0.044	1.281	0.066	0.044
	75-63 $\mu\text{m}$	47.545	0.5	27.741	3.215	0.983	15.982	0.045	1.357	0.059	0.045
	63-53 $\mu\text{m}$	47.704	0.502	28.702	3.463	1.031	16.237	0.047	1.406	0.059	0.047
	53-45 $\mu\text{m}$	46.281	0.516	19.954	4.343	0.731	14.006	0.053	0.965	0.046	0.053
	45-25 $\mu\text{m}$	45.636	0.513	15.94	4.262	0.548	12.431	0.056	0.843	0.049	0.056

**Figure 3.19 Spidergram of anorthositic-suite for comparison of major oxides between earth and moon**

From the spidergram (Figure 3.19) it may be well observed that the lunar regolith has more silica compared to the terrestrial rocks and it may also be observed that the Ca and Al<sub>2</sub>O<sub>3</sub> components of the plagioclase formation is more than the mafic for both the rocks types.

### **3.8.1.2 Comparison of Lunar Mare regoliths and Lonar simulant, soils and ejecta**

Apollo and Luna return samples had mare soils from its landing sites. Since the detailed petrographic properties of lunar soils, particularly the finer fractions are poorly known (Taylor et al 2001). To study the properties of lunar mare soil Apollo return sample 15041-94 published data was taken and correlated with the Lonar ejecta, soil and pulverized (simulant) sample.

Taylor et al (2001) examined the properties of the size fractions or individual soils reveal interesting and highly significant systematic changes. There is an increasing impact-produced agglutinitic glass content with decreasing grain size. The modal abundances of crystalline plagioclase are relatively constant to slightly increasing with decreasing grain size of the fractions. However, the abundance of all other component (pyroxene, oxides, volcanic glass and olivine) decrease in the particle size. This decrease of pyroxenes is pronounced very significant since pyroxene probably the most optically active of the lunar minerals. Also that impact-produced soil contains naophase Fe<sup>0</sup>. An important conclusion is that the abundance of plagioclase increases relative to the mafic minerals with decreasing particle size. These effects would seem to be a function of the agglutination process and that of selective comminution, experimentally verified by (Cintala and Horz 1992).

The Lonar soil in hand specimen samples are dark reddish brown to black in colour, earthy with vitreous lustre, few rock pieces are found mixed with it formed due to weathering of basalts (country rocks). Impact-derived melt rock fragments and glasses are common in the ejecta deposits up to about a crater radius from the crater rim and in the soil that is probably derived from the weathering of the ejecta (Nayak 1972; Fredriksson et al 1973; Ghosh and Bhaduri 2003). The matrix consists of finely pulverized

basalt (Wright 2008). In hand specimen they are generally, white in colour with few basalts clasts.

From the basalt simulant (powdered) samples also show the composition variation systematic similar to that of the Lunar soil. As the grain size decreases the plagioclase increases and while the pyroxene and the olivine too decreases. However, the lunar soil contains the naophase  $\text{Fe}^0$  which is not a part of the simulant.

Ejecta of any crater is an important factor. The way in which ejecta is spread tells about the angle of impact. Spreading pattern for ejecta talks about degree of fluidisation of the rock. This pattern also depends on the planet gravity and presence or absence of atmosphere. Thus if we know how these parameters effect spreading of ejecta then we can conclude about the conditions of impact on that particular planet. And the best place to know these parameters is our earth itself. However, hardly a few craters on the earth are studied well with reference to this point. Lonar crater has surprisingly well-preserved ejecta. Thus, these ejecta should be studied further and then it should be conserved also. The ejecta samples were collected from each direction (N,E,S,W) of the crater and geochemical data is provided in Table 2.

This ejecta blanket is spread over about 1350m away from the crater rim and slopes away by 2-6 degrees. The uppermost region of ejecta contains the deposits that were melted due to the impact. The ejecta blanket also outcrops in small gullies, unlined wells, building foundation pits, trenches, and quarries. The ejecta blanket grades from overturned stratigraphy with brecciated units of several m sizes to unsorted clasts in a coarse matrix in the outer continuous ejecta (Stewart 2005). The matrix consists of finely pulverized basalt (Wright 2008).

In this study, soil samples were collected near the ejecta in the Lonar region and a comparative study was made between the soil, ejecta and the target rock. Since not much details of the soil near the ejecta are available.

The diagram 3.20 (also from Table 3.7) show that the SiO<sub>2</sub>, Na<sub>2</sub>O and K<sub>2</sub>O are similar, slightly lower Al<sub>2</sub>O<sub>3</sub>, Fe<sub>2</sub>O<sub>3</sub> and MnO and high CaO were observed for ejecta and MgO is lower for soil, while the TiO<sub>2</sub> is slightly higher for the target basalt. The soil/paleosol samples from several areas around the crater represent a much more advance state of chemical evolution than the ejecta samples, which are probably much younger (Newsom 2007). The contrasting chemistry of the ejecta suggests a much less advanced state of alteration, but still representing a substantial difference from the target rocks. The physical process of creating the large volume of fine-grained matrix material present in the ejecta may be the most important aspect of promoting chemical alteration by aqueous processes. The presence of caliche, a carbonate-rich material at the best of the impact deposits supports the role of leaching and chemical transport. Hence, the ejecta are enriched in the CaO content than the soil. Additional work on the detailed mineralogy of the altered ejecta will help address this issue. Having studied the Lonar rocks, ejecta and soil, these are compared with the lunar mare basalts, which are considered as analogues.

Taylor et al (2001) selected nine lunar mare soils from the Apollo 11,12,15 and 17 sample collections. The soils were sieved and sizes fractions <45µm, 20-45 µm, 10-20 µm, and < 10 µm was separated. Bulk chemistry was determined using electron microprobe and based on the Ti content they were segregated as high-Ti and low-Ti mare soils. They observed that the mare soil samples have systematic differences among one another, as well as among the different grain-size fractions.

To understand the lunar regolith, in this study an attempt has been made to compare the geochemistry of lunar soil grain-size fraction and Lonar ejecta, soil and the basalt powder (simulant) was carried out. The Lonar ejecta bulk chemical composition of the size fractions of Lonar ejecta, soil and powdered sample and also Lunar mare soils 15041-94 (Taylor et al 2001).

From the Table 3.7 it may be observed that there is not much difference between the four types of materials compared here. The ejecta samples and soil/paleosol samples are almost similar to the target basalts. The ejecta are enriched in CaO content while the lunar mare soils have more MgO content.

To understand the relationship between the grain sizes and chemical composition bar diagrams (Figure 3.20 a-j) were plotted.

From the diagram it was observed that the lunar simulant basalt powder shows almost similar chemical composition to lunar mare soils. However, MnO, MgO and TiO<sub>2</sub> (<53 $\mu$ m decreases) increases while for the lunar soil it decreases.

The laboratory samples are sized for up to 25 $\mu$ m only and the lunar are <10 $\mu$ m. Further studies will be made on much finer grain sizes.

**Table 3.7 Major oxide wt (%) of lunar mare regolith and simulant**

Sample		Size ( $\mu\text{m}$ )	$\text{SiO}_2$	$\text{Al}_2\text{O}_3$	$\text{Fe}_2\text{O}_3$	Mn O	Mg O	$\text{CaO}$	$\text{Na}_2\text{O}$	$\text{K}_2\text{O}$	$\text{TiO}_2$	$\text{P}_2\text{O}_5$
Lunar	Ej(4)	90-75	49.86	13.38	12.81	0.16	4.26	12.01	1.53	0.36	1.53	0.22
		75-63	50.16	13.45	12.96	0.17	4.51	12.92	1.57	0.37	1.72	0.23
		63-53	47.37	12.31	12.54	0.16	2.79	11.51	0.97	0.31	1.52	0.14
		53-45	44.77	11.40	11.49	0.15	1.56	9.19	0.66	0.18	1.12	0.04
		45-25	44.29	11.30	10.92	0.14	1.23	4.67	0.63	0.08	0.65	0.02
	Sol (1)	90-75	50.06	13.61	14.02	0.22	4.13	7.51	0.94	0.46	2.26	0.19
		75-63	50.69	13.92	13.64	0.21	4.39	8.07	1.05	0.47	2.20	0.20
		63-53	50.38	13.78	13.69	0.21	4.15	8.29	1.05	0.45	2.17	0.19
		53-45	45.23	11.63	12.13	0.17	1.52	5.44	0.69	0.20	1.25	0.05
		45-25	45.55	11.75	11.98	0.15	1.84	9.23	1.01	0.18	1.16	0.07
Lunar	Basa lt	90-75	49.57	13.33	13.41	0.19	5.66	10.15	1.67	0.36	1.99	0.20
		75-63	50.67	13.92	13.52	0.19	6.75	10.96	1.99	0.34	1.83	0.22
		63-53	50.81	14.01	13.25	0.19	7.06	11.06	2.09	0.31	1.87	0.22
		53-45	51.41	14.09	13.60	0.20	8.22	11.31	2.24	0.30	2.21	0.23
		45-25	51.11	14.16	13.30	0.20	7.51	11.30	2.21	0.31	2.00	0.22
	1504 1-94	<45	46.40	13.50	14.20	0.20	10.8 0	10.30	0.41	0.19	1.83	0.21
		20-45	46.10	12.50	15.20	0.20	11.2 0	9.91	0.36	0.16	2.03	0.19
		10-20	46.20	13.50	14.40	0.21	10.8 0	10.20	0.41	0.18	1.88	0.24
		<10	46.60	16.40	11.00	0.17	9.37	11.60	0.49	0.23	1.79	0.20

From the Table 3.7 and Figure 3.20 it may be observed that there is systematic difference in the geochemistry. With decreasing grain size, FeO, MgO, and  $\text{TiO}_2$  concentration decreases for ejecta, soil. While  $\text{CaO}$ ,  $\text{Na}_2\text{O}$ , and  $\text{Al}_2\text{O}_3$  (plagioclase component) increases for all soils.

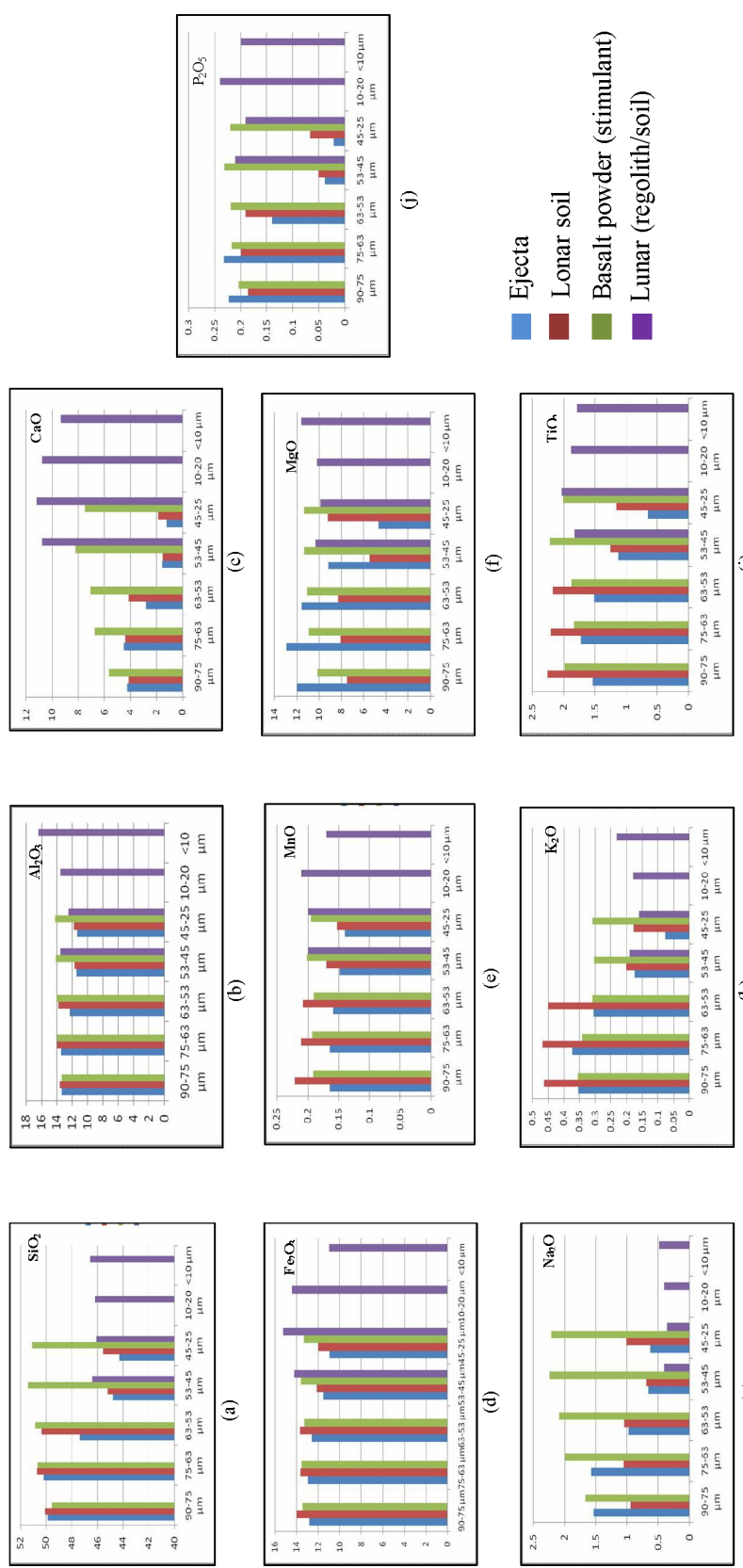


**Figure 3.20 a-j Correlation of geochemistry between Lunar mare soil 15041-94 and Lonar ejecta, soil, basalt powder (simulnat).**

### **3.9 METEORITC COMPONENT STUDY**

Lunar crustal samples collected during the Apollo program, and as lunar meteorites, contain both ample physical (Day et al 2006), and geochemical evidence for impactor materials with generally chondritic and, in some cases, iron meteorite-like characteristics (Higuchi and Morgan, 1975: Hertogen et al 1977: Korotev, 1994: Norman et al 2002: Puchtel et al 2008). The process that brought FAN and MGS rocks to the lunar surface was meteorite impact, so it is possible that all samples have been contaminated by meteoritic materials (Day et al 2010). Having understood the importance of the meteoritic study in lunar science it was decided to study the meteorite in this thesis.

#### **3.9.1 Sulagiri Meteorite**

Meteoritic samples collected from the impact site weigh 5g. Macroscopically (Figure 3.21a and b) the exterior has light grey coloured on broken surface, with black patch or burned surface that occurred when the meteorite entered the earth's atmosphere. This part of the sample helps the meteoritic origin. The grain size varies from 1cm to 1.5 cm, pyroxenes are pale coloured, olivines are brown coloured and few plagioclase feldspars can be readily recognized. The sample appears fresh as it was recovered immediately after the fall (hence no weathering).

The thin section (Figure 3.21c) was prepared with the available facility (not in vacuum chamber) shows that the meteorite has dark matrix as ground mass with phenocrysts of mostly orthopyroxene and olivine. Clinopyroxenes are rare. Troilites (FeS) are more frequent than iron metal present in moderate amount. Feldspar grains are few and are clouded. Chondrules are poorly developed can be identified from the thin section. The chondrules are homogenized with coarse to moderately recrystallized matrix

indicating high equilibrated petrographic type, based on the mineralogy and chemical composition the Sulagiri meteorite is classified to LL class and the metamorphic grade 6 with shock stage is S2 (Murty 2009).

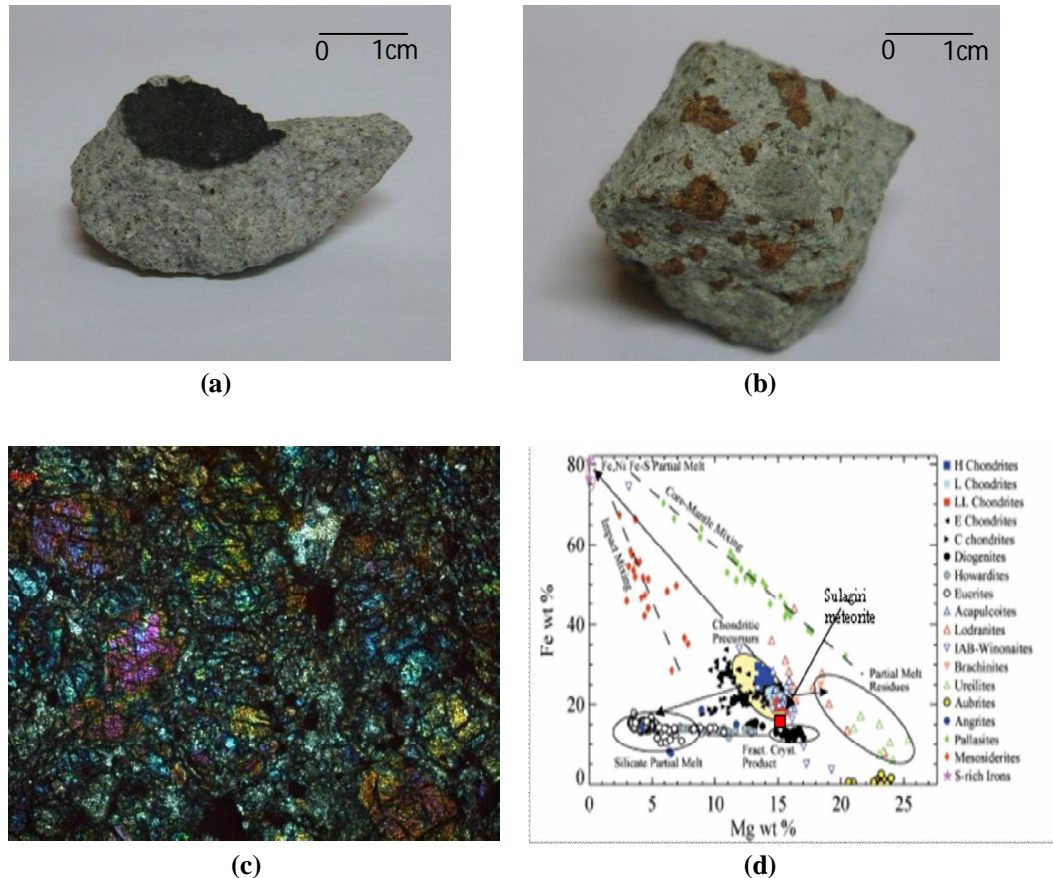


**Figure 3.21 (a,b) Photos of Sulagiri meteorite (c) thin section photo (d) Classification using Nittler et al (2004).**

### 3.9.2 Cosmochemistry

Iron and magnesium are two of the most useful major elements to determine both meteorite groupings and geologic processes. Their concentrations within mafic silicates vary systematically throughout the solid solution series (fayalite to forsterite, enstatite to ferrosilite). Magnesium is partitioned solely into mafic silicates in most meteorites, while iron occupies

a variety of valence states and occurs in mafic silicates, metal and sulfides. Urey and Craig (+3/-) first used the concentration of total iron to delineate chondrite groups.

Chondritic meteorites exhibit a range of iron ( $\sim$  18-34 wt%) and magnesium ( $\sim$  8-16 wt%) concentrations. Ordinary chondrites exhibit a trend of decreasing magnesium with increasing iron in the order LL  $\rightarrow$  L  $\rightarrow$  H, although some scatter exists within these groups. (Note that some care must be taken when considering absolute abundances, as opposed to abundance ratios. Much of the change in the Mg along this sequence is due to the need to measure abundances in relation to the total mass of a rock: as the wt% of Fe goes up, the fractional abundances of other elements must go down. In fact, the Mg/Si ratio is basically identical for L and LL chondrites, but slightly higher for H chondrites.) Carbonaceous chondrites exhibit a trend of increasing Mg concentration with increasing Fe concentration in the sequence CI  $\rightarrow$  CM  $\rightarrow$  CR  $\rightarrow$  CO  $\rightarrow$  CV  $\rightarrow$  CK.

This trend reflects both changes in modal mineralogy and the decrease in water content from CI to CM to the dominantly anhydrous carbonaceous chondrite groups. The latter point is supported by the general trend of increasing H concentration with decreasing Mg concentration in the same sequence. Not surprisingly, EH chondrites have higher Fe and lower Mg abundances than do EL chondrites, reflecting higher metal and/or sulfide abundances in EH compared to EL chondrites. The only R chondrite in our database, Rumuruti (Jarosewich 1999), plots within the range of H and CR chondrites.

**Table 3.8 Major oxides concentration (wt.%) of Sulagiri meteorite**

<b>Major oxides</b>	<b>wt (%)</b>
SiO <sub>2</sub>	36.74
Al <sub>2</sub> O <sub>3</sub>	0.8
Fe <sub>2</sub> O <sub>3</sub>	33.39
MgO	22.28
CaO	2.55
MnO	0.37
Na <sub>2</sub> O	1.28
K <sub>2</sub> O	0.12
TiO <sub>2</sub>	0.16
P <sub>2</sub> O <sub>5</sub>	0.36

In this study meteorite cosmochemical analysis were carried out at NGRI and Table 3.8 provides the data, of the Sulagiri meteorite.

The SiO<sub>2</sub>=36.74%, Fe = 20.11, Mg = 15.59, CaO= 2.55%, and low Al<sub>2</sub>O<sub>3</sub> (0.80%). In order to understand the classification of the Sulagiri meteorite, a plot was made on classification diagram published in Nittler et al (2004), where the authors define the Chondritic meteorites exhibit a range of iron ( □ 18-24 wt%) and magnesium ( □ 8-16 wt%) concentrations (Figure 3.12e) . Ordinary chondrites exhibit a trend of decreasing magnesium with increasing iron in the order LL → L → H, although some scatter exists within these groups.

### 3.10 CONCLUSION

The lunar samples have provided our only direct information about the moon's minerals, chemical composition, and age. Lunar rocks have also provided information about the moon's origin, the evolution of its crust, and the timing of critical events such as volcanism and meteorite bombardment (Heiken et al 1991).

The calcic plagioclase for both lunar and terrestrial high-Ca anorthosites shows textural evidence of exsolution indicating igneous origin (Irving et al 1974). Chemical compositions of Archean anorthosite are similar to that of lunar anorthosite (Ashwal 1993).

The Dunites are Mg-rich in both Lunar and Chalk hills, The Lunar and Lonar basalts belong to tholeitic magma. The simulants and regoliths are almost comparable. The Sulagiri meteorites belong to LL 6, ordinary meteorite.

It may be observed that the compositional (mineralogical and chemical) similarity between the lunar return samples and the terrestrial rocks indicate that Sittampundi anorthosites, Chalk hills dunite and Lonar basalts can be called as analogue rocks to the moon.